Politecnico di Torino

Master's Degree in Automotive Engineering
Accademic Year 2023/2024
March 2024

Master's Degree Thesis

e-Scooters Steering Angle: Design and Realization of a Measuring System

Advisors:
Prof. Alessandro Vigliani
Ing. Angelo Domenico Vella

Candidate:
Giulio Maria Paggiola

Politecnico
di Torino

Index

Tables index

Figures index

1 Abstract

By having a look at the means of modern transportation, electric kick-scooters are becoming more and more popular, thanks to the fact that a lot of companies started to provide a sharing service increasing so the spread of the micro mobility. Even if their popularity is daily growing bigger, few studies are brought to the scientific community.

Aim of this work is designing and realizing a steering angle measuring system capable of improving the understanding of the lateral dynamics of this kind of vehicles, following recent studies on their longitudinal dynamics [1].

Through the usage of CAD software like the one used for this purpose, Solidworks, and through various kind of manufacturing processes, is indeed possible to realize an ad-hoc system that can be adjusted to the needs of the researcher.

2 Introduction

After intense investigation, no evidence was found regarding the analysis of these two-wheeled vehicles (2WV), even though their widespread usage should have led to further studies to better understand criticalities and possible improvements.

However, a first approach could be represented by a preliminary analysis on other types of two-wheeled vehicles, in the hope to find more useful literature. Indeed, referring to bicycles and motorcycles, some studies have been done and so they could be consulted. As an introductive part to this thesis, this paragraph is intended to give a quick glance at the current state of the art of the knowledge regarding the two wheeled vehicles. Particular attention has been paid to focus on the longitudinal and lateral dynamics of the above-mentioned vehicle.

An interesting study that has been a major contributor in the contents of almost every other paper on the subject is “Steering and straight running behaviour” of Sharp.

Reading such a writing, and looking at the proposed 2WV dynamics, it is immediately clear that steering plays a major role

in the understanding of any kind of manoeuvre: having a single-track vehicle model (STM) implies unstable behaviour [2], controllable only by acting on the vehicle commands, one of which, if not the most important, is the steering one.

The steering control can be assumed as one of two types:

- Fixed control: actions performed on the steering angle (e.g. leaning of driver's upper body);
- Free control: actions performed on the steering torque (e.g. leaning torque).

For both controls, the leaning behaviour is crucial, and the higher the ratio between the Rider's upper body mass and the Machine mass is, the higher is the importance of the leaning.

By the way, since the steering angles in normal operations are always considerable very small, the fixed control type of steering has almost no relevance in practice.

The study on the 2WV dynamics reveals that the most important parameters in the understanding a model of the system are:

- Roll angle;
- Yaw angle;

- Longitudinal coordinate;
- Lateral coordinate.

For what concerns the tires forces exchange, the study involves a linear combination of sideslip and camber angles, with an intense use of the Pacejka magic formula. An important characteristic is that lateral forces have found to be lagging the angles considering a first order characteristic: the force production is in fact not instantaneous after the tires deformation, there is instead a considerable delay between the two events [3].

At high speeds, that are not considered in the case of electric kick-scooters, aerodynamic forces significantly alter the tires forces, leading mainly to a worsening of the weave mode (the act of overall vehicle rotating on its vertical axis).

This influences at high speed are commonly attenuated by installing steer-dampers, also capable to reduce eventual wobble modes (rotation of the front wheel around its steering axis at frequencies higher than the ones a driver could handle).

Another aspect that should be considered, is the last of the three main modes characterizing the 2WV: the capsize.

The capsize mode represents the lateral rollover of the vehicle, mainly affecting it at very low speeds (but not only).

This mode is less dominant at increased longitudinal accelerations, thanks to the roll/yaw inertia coupling effect.

However, finding a way to dig deeper into this matter results quite obviously in having a look at experimental procedures and analysis. One important document that very well deals with this concept is “Experimental study of motorcycle transfer function for evaluating handling”, by Biral.

Looking at the cited common experimental setups, involving (almost always) null longitudinal accelerations, the range of values for the considered variables are practically always the same, here reported in Table 1.

Table 1 Variables range

Variable	Range	Unit of measure
Steering angle	± 30	°
Roll angle	± 45	°
Yaw rate	± 30	°/s
Lateral acceleration	± 1	g
Rider lean angle	± 20	°
Rider pitch angle	± 30	°

Interestingly, for all the considered different experimental procedures, no discrepancies were found in the choice of such intervals.

A very important parameter was found to be, specifically at low speeds, the tires lag, affecting the overall vehicle dynamics. These are often taken into account by the Relaxation Models [4].

Regarding the experimental procedure and setup, a common performed test is the so called “Pulse Steer Torque”, in which the steering torque input is performed suddenly, in the briefest time possible. Such test leads the coupling pitch/lateral acceleration: the higher the lateral acceleration is, the higher the pitching behaviour becomes. Noticeably, if the pitch frequency reaches the weave frequency boundaries, a dangerous phenomenon occurs: the cornering weave, where the vehicle becomes uncontrollable, entirely rotating on its vertical axis while in bending. A solution has been found in an enhanced dampening of the rear portion of the structure.

Moreover, the Pulse Steer Torque method is not the only one in order to excite some vehicle’s modes or to study the whole

dynamics [5]; in fact, other common test procedures, as can be found in “Development of handling test procedures for motorcycles” by Zellner, comprehend:

- Steady State Turn: performed at different speeds and cornering radii, usually used to measure the gain-ratio output/input of the vehicle controls (low frequency response);
- Constant Steer Torque: as expected, the input is set and unchanged;
- Constant Roll Angle: one of the least accurate, includes a monitoring display that the driver uses to match the current roll angle to a pre-defined value. The main outcome is the relation between speed and steering torque (the required torque decreases at increasing longitudinal speeds);
- Single Lane Change: at different lane spacings and speeds (transients’ analysis);
- Double Lane Change: more pronounced transients are here considered.

All these types of tests excite different behaviours, but generally, as previously said, the main modes of 2WV that differs from the

ones characterizing the automotive field are the most common. The main modes that mostly lead the dynamic behaviour are not in fact exclusively Roll, Pitch or Yaw, but are instead the Weave, the Wobble and the Capsize [3]. As a supporting reading, “Theoretical and experimental investigations of motorcycle dynamics” by Verma is a well-accepted choice.

Speaking of Weave, Wobble and Capsize, details are now proposed.

The Weave is often characterized at low frequencies (relative to the vehicle excitation range), up to 3 Hz, both at high and low speeds. By considering a driver not leaning at all, this mode is encountered only at high speeds.

The Wobble, by contrast, is excited at high frequencies (too high for the rider to be dampened) in the range 8/9 Hz. A stiffening of the front frame is often required to avoid this dangerous effect.

The Capsize is instead a non-oscillatory behaviour obtainable for both very low or very high speeds. Having a divergent characteristic, the steering input and the roll angle must be constantly adjusted to avoid rollovers.

While the steady-state aerodynamic forces seem to not affect the stability of the system, transient and unstable aero-forces

strongly destabilize the dynamics, mainly acting on the rear frame of the 2WV, suffering from strong flexibility or lack of structural stiffness (it would not seem the case for electric kick-scooters).

Coming back to the experimental procedures to obtain valid data to analyse such dynamics, even if the most common test procedures have been briefly introduced, also the “Slalom Test” deserves its place in this list. In any case, note that at the present time, it has to be considered outdated, since it will be later discovered that it has intrinsic and strong limitations.

However, according to literature, the correlation between experimental and simulation data is always performed considering as a model the Sharp proposal [6], either in its standard form or slightly changed.

By the way, the Slalom test aims mainly to evaluate the transfer function related to the Roll angle and Steer torque ratio. It has been proved that the velocity for which the transfer function $\frac{\varphi}{T}$ (roll angle/steering torque) is maximized, is experienced by different drivers as “Good Handling” [7].

Following Suyizaki results [7], by analysing the Power Spectral Density of the roll angular velocity ($\dot{\varphi}$), a lower yaw rate lag led to the abovementioned "Good Handling".

Studying the PSD revealed the intrinsic limitations: a test like this one would excite the vehicle only at frequencies equal to the ratio between the forward speed and two times the pitch of the slalom cones (Figure 1, $f_s = \frac{\dot{x}}{2p}$).

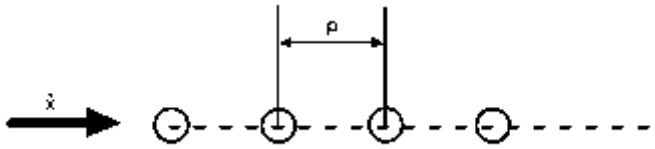

Figure 1 Slalom course

By contrast, all tests performed at different speeds and pitches, resulted in a very small range of speed for which the transfer function $\frac{\varphi}{T}$ would be maximized: considering in-phase torque, the TF would be maximized always at 7/8 m/s, leading to the feeling of good handling for any driver.

The outcome of such analysis permitted to understand that lower steering torque resulting in higher roll angles would be perceived as better by the riders, in contrast to various hypothetical reasonings.

Such hypotheses rely strongly on lumped parameters models and linearized and simplified approximations. Various approaches are totally plausible, but the one fo the most valid is certainly the one proposed by Cheli in “Numerical and experimental approaches to investigate the stability of a motorcycle vehicle”.

In this case, the vehicle itself, considering the already introduced modes, can be approximated by an assembly of rigid bodies mainly for two coupled reasons:

1. The vibration modes (Wobble and Weave) comprised between 1 and 10 Hz are rigid ones.
2. All the handling phenomena exist below the 12 Hz threshold.

What really affects the results is the geometry of the vehicle and the stiffness of the two main frames: the front frame and the rear one [8].

In the effort to obtain a correlation between experimental and simulation results, these rigid bodies are implemented in a variety of software. Most of the time, after having defined a lumped parameters model, the aim is to try to find an appropriate control method to provide the best and most realistic results.

A common approach is using LQR methods and Luenberger observers, simulating a steering control working on the lean error angle by using as input the most important parameter: the steering torque [9].

Through validation, is found that steering torque is never null (in reality it can be null only in case of sign change), even in straight-running cases. One of the causes (other than the capsize mode excitation) can be found in the a-symmetry geometry of 2WV.

For what concerns electric kick-scooters, this concept should be either proved or discarded.

The rigid bodies used to define the model of the 2WV, as said before, all rely on the 71 Sharp model [6]. The validation of the simulation environment by means of experimental procedures surprisingly revealed that a 2 Degrees of Freedom (DOF) model can significantly well-approximate a 29 DOF model [10]. Such a discovery permits to save calculation time and effort, affirming the robustness of such a simplified model on which anyone can rely.

Focusing instead on e-scooters, starting from these premises, further studies can be conducted considering that most of the problems related to motorcycles are here absent, like high

speeds or a-symmetry to name a few. The low-speed operations, the small angles which the vehicle undergoes and the possibility to experiment a various number of conditions, all lead to the possibility of studying the scooter dynamics in a easier way with respect to motorcycles.

Almost all the conditions that are met in experimental procedures could also be linearized, since the range of values that the main parameters undergo are strongly far away from their non-linear ranges. As an example [11], roll angles up to 45° can be considered as stable and, in theory, can be deducted linearly. This is particularly true speaking about scooters in place of motorbikes.

The only problematic foreseen in the experimental procedure is the impossibility of measuring the steer torque due to the lack of instrumentation. By contrast, through a process of design and engineering, the vehicle used in the experimental tests can be adapted to the mounting of various other sensors like accelerometers, an IMU (Inertial Measuring Unit), an optical encoder and a steering angle sensor.

In the current study, the vehicle on which the design process has been conducted is a Xiaomi Pro 2.

According to the producer, the Xiaomi Pro 2 e-scooter (Figure 2) is characterized by an aeronautical aluminium grade structure weighting 14.2 kg (net weight): for a vehicle equipped with a 446 Wh battery pack, this is a very promising result.

Such battery pack provides a range of 45 km by using the 0.6 kW in-wheel motor, capable of overcoming slopes up to 20%, with a maximum speed of 25 km/h (electronically limited for safety reasons). Moreover, the scooter is provided with KERS, a proprietary regenerative braking system, used to enhance the vehicle's autonomy.

The wheels are both mounting 8'' tires and present disc brakes controlled by an electronic ABS system to accomplish the reach of best braking space.

Figure 2 Xiaomi Pro 2 [12]

3 Hardware Setup

Given this general information about the vehicle, the issue on how to monitor the steering dynamics rose up.

Since the steering angle plays a major role in the lateral dynamics of any vehicle, its measurement is of great interest. The scooter, unlike common bicycles or motorcycles, does not present a frame structure suitable for a plug and play usage of angular sensors. In order to acquire the useful measurements, an acquisition setup has to be designed.

By the study of the e-scooter CAD-implemented model, through the usage of SOLIDWORKS software, a preliminary design is conducted.

The first problem is the choice of the sensor that must be mounted: in this case, an angular potentiometer seemed the most suitable option. A detents-less angular potentiometer is chosen to eliminate the problem of its rotational range.

The second problem relies in how to transmit the motion of the steering column (rotating as a whole) to the potentiometer shaft: a pulleys-belt system is designed, permitting to have a continuous reading by means of a reduction equal to the dimensional ratio between the pulleys (one driven and one driver).

Having solved the first two problems, the interface between the driver pulley and the steering column must be faced. The steering column is indeed characterized by an elliptical shape, and not by a circular one. However, its axis of rotation coincides with the one of the ball bearings permitting the motion, meaning that a simple assembly can be mounted around the stem to convert the section from elliptical to circular.

Once this assembly has been mounted, orienting its design to a multi-purpose usage, it is possible to use it directly as the driver pulley.

Then, by attaching a bracket to the front section of the fixed deck column, the potentiometer and driven pulley system can be mounted accordingly to the driver pulley position.

Being able to transmit the motion from the steering column stem to a fixed position angular potentiometer permits us to read the steering angle by converting a voltage signal matching the angular position of the potentiometer shaft to its impedance behaviour. Steering the scooter results in a potentiometer shaft rotation, hence resulting in an impedance variation. Increasing or decreasing impedance leads to a different voltage reading that, once sufficient experimental data is acquired, can be translated into an angular variation.

3.1 Driver Pulley

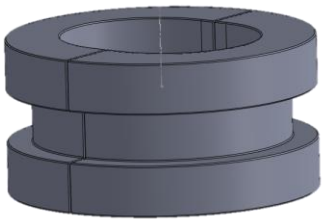

Figure 3 Driver pulley

This pulley, depicted in Figure 3, is intended to be made of two symmetrical pieces fastened together through screws. It is fixed to the steering stem, and it accomplishes two tasks:

1. It converts the section from elliptical to circular.
2. It accommodates the belt allowing to transfer the rotation to the fixed potentiometer system.

3.2 Driven Pulley

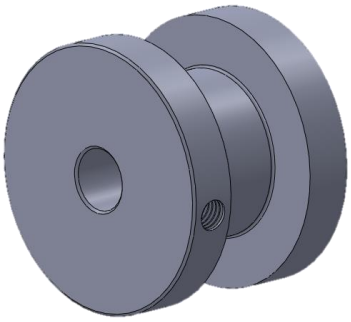

Figure 4 Driven pulley

The pulley in Figure 4 is instead mounted onto the potentiometer shaft, receiving the motion from the steering column stem.

3.3 Potentiometer

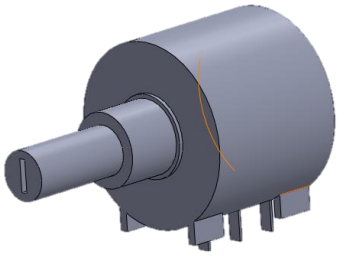

Figure 5 Angular potentiometer

As previously mentioned, this potentiometer (Figure 5) does not present any detent, meaning that the shaft can freely rotate in both directions, clockwise and anti-clockwise. The choice prevents any problem in finding any end stop between the steer rotations.

3.4 Bracket

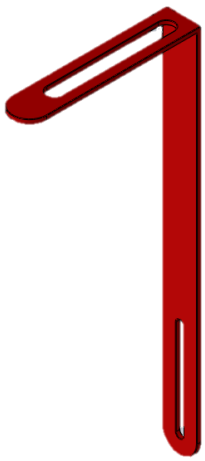

Figure 6 Bracket

The bracket is the element that permits the fixing of the potentiometer assembly to the fixed frame of the scooter. Its slots are designed to accommodate adjustments in both local-longitudinal and local-vertical direction to keep the belt always in tension (Figure 6).

The bottom portion is fixed to the scooter deck, while the upper section is the interface between the fixed reference and the potentiometer.

3.5 Mounting Plate

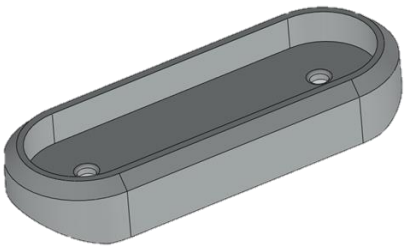

Figure 7 Mounting plate

The plate interposes between the bracket and the deck, offering a flat contact surface instead of the elliptical one that would otherwise be provided (Figure 7).

3.6 Complete Setup

Once all the components are mounted, the setup is presented as follows in Figure 8:

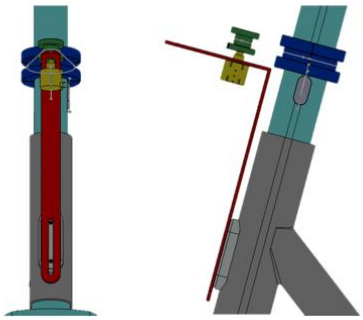

Figure 8 Front and lateral views of the complete setup

Analysing the picture, it is possible to individuate the single components following the presented colour-scheme:

- Potentiometer: Yellow
- Driven Pulley: Green
- Leading Pulley: Blue
- Bracket: Red
- Mounting Frame: Light grey

The belt connecting the pulleys is instead represented by the software Belt-Feature, here depicted as light grey continuous line running through the setup.

A detailed view of the belt connection is here provided in Figure 9:

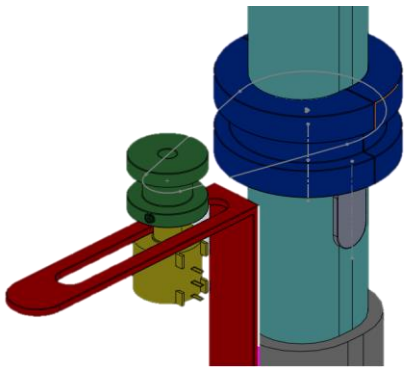

Figure 9 Isometric view of the belt connection

3.7 Revising Geometry

After searching for the proper belt to transmit the motion, the choice changed towards belts without any rib.

To obtain smooth operations and a consistent transmission, the pulleys were re-designed to better accommodate the new type of belt. A V-tapered geometry seemed the best to accomplish such task.

Also, the fastening method for the two-parts pulley (driver) was implemented.

The new setup looks Figure 10:

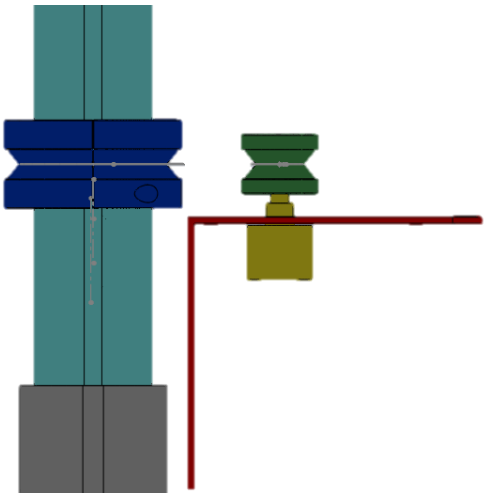

Figure 10 Local lateral view of the new setup

The two-pieces driver pulley, with the newly implemented threaded holes:

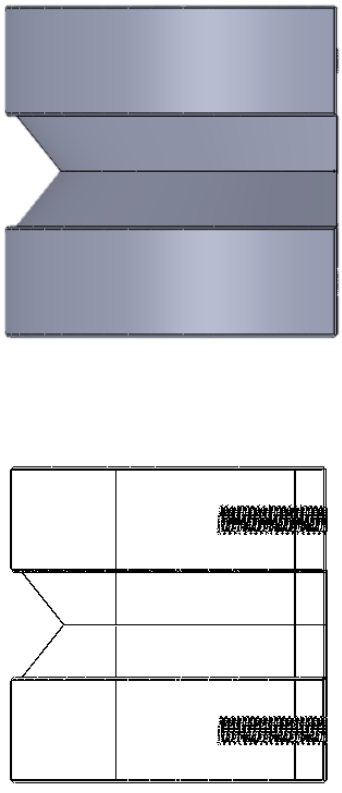

Figure 11 Left views of driver pulley

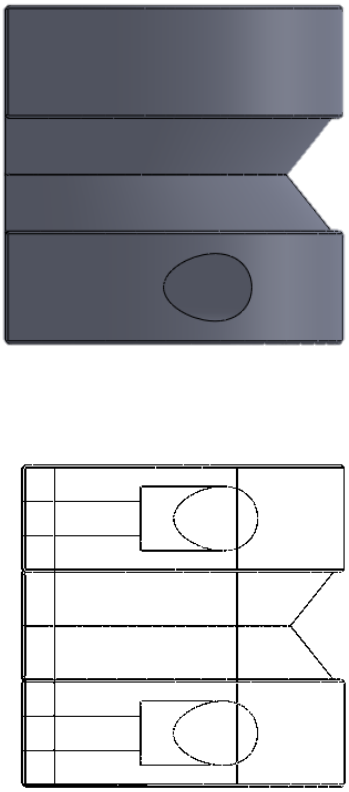

Figure 12 Right views of driver pulley

To better understand the holes positioning, intended to accept M3x0.5 screws, Figure 13 and Figure 14 are presented:

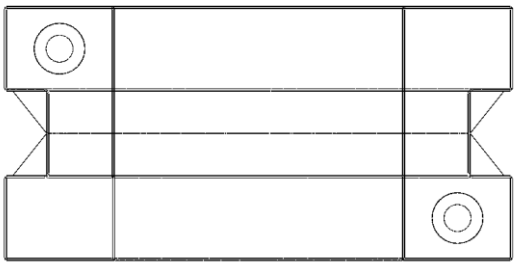

Figure 13 Left part

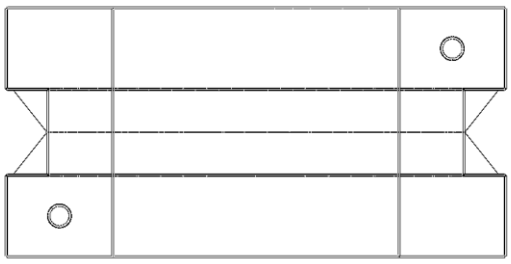

Figure 14 Right part

According to what has been changed in the driver pulley, also the same revolving features were implemented in the driven pulley, Figure 15:

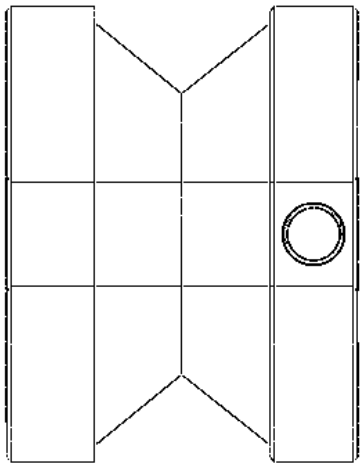

Figure 15 Driven pulley

3.8 Beltless Design

A different design has been finally considered, one that would not require any belt-transmission system. Aiming for robustness and reliability, this setup will be the actual one when it will come to the actual realization.

The motion is transmitted through a swinging arm mounted on the potentiometer shaft. This component creates a prismatic joint in which a threaded rod can linearly move. The linear movement is child of the rotation of the rod connected to the bracket fixed on the driver pulley (around a different axis with respect to the potentiometers shaft).

The basic structure fixing the potentiometer to the deck remained the same while the moving elements drastically changed.

The driver pulley has been flattened on its frontal surface to accommodate the fixing points for a bracket, as it can be seen in Figure 16.

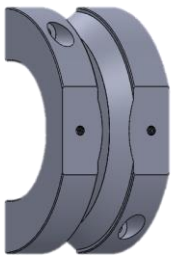

Figure 16 Flattened driver pulley

The swinging arm is instead freshly designed: the central slot permits the rod to move linearly, solving the problem concerning the distance between the rotation centres of both the steering stem and the potentiometer shaft, as it can be clearly seen in Figure 17. Indeed, the absence of a longitudinal slot would not permit the rotation of the stem since the rod would be constrained in place.

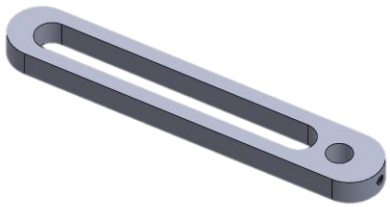

Figure 17 Swinging arm

The overall setup, considering that only the upper part has been changed, is here shown (Figure 18 and Figure 19):

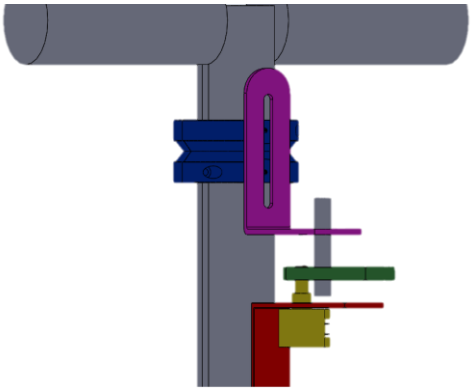

Figure 18 Beltless setup (1)

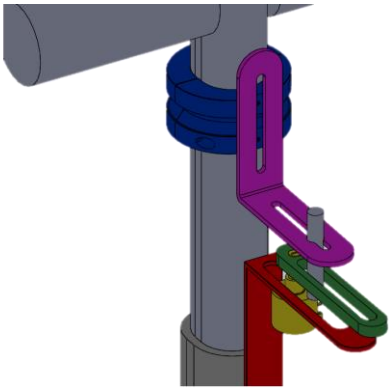

Figure 19 Beltless setup (2)

Once rotated the steering column, it is possible to see how the swinging arm permits such a movement (Figure 20).

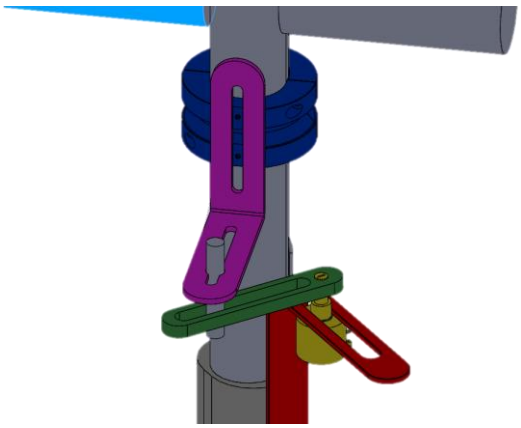

Figure 20 Beltless setup, rotated

However, such a system introduced the problem of relating the angle of steering to the angle of rotation of the potentiometer shaft.

Initially it has been tried to find an analytical relationship between the two angles (Equation (1)**Error! Reference source not found.**). Noticeably, finding the angle of the potentiometer from the steering angle resulted analytically possible, while finding the inverse relationship required a numerical approach. Basing the calculation on the parameters presented in Table 2, it is so possible to derive useful expressions like Equation (2).

Table 2 Geometrical parameters, sketch

Parameter	**Value**
R (Axis-Rod distance)	83 mm
α	Steering angle
β	Potentiometer angle
D (Axis – Axis distance)	63.36 mm

$$\cos(\alpha)\tan(\beta) - \sin(\alpha) = \frac{D}{R}\tan(\beta) \quad (1)$$

$$\cos(\alpha)\tan(\beta) - \sin(\alpha) = \frac{63.36}{83}\tan(\beta)$$

(2)

Calling β the angle of the potentiometer shaft and α the steering angle, the kinematics can be portrayed as follows in Figure 21:

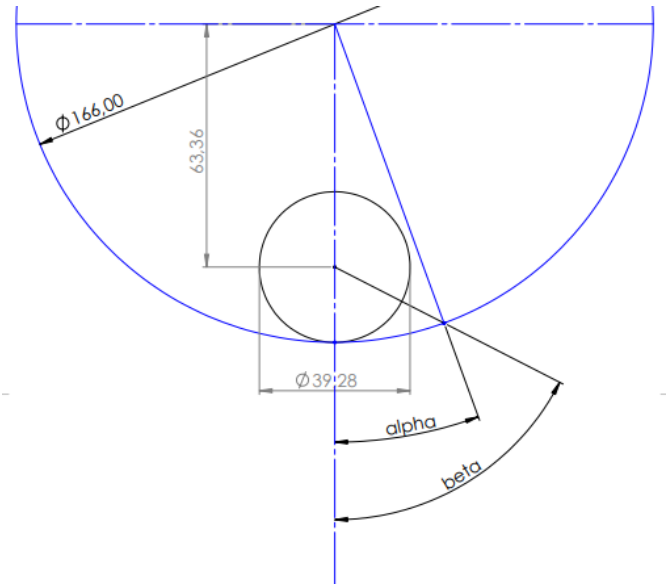

Figure 21 Beltless design kinematics

In Figure 21, the 166.00 mm semicircle represents the trace of the rod rotating around the steering column axis; the smaller black circumference (ϕ39.28 mm) represents the trace of the contact point at 0° between the rod and the swinging arm.

From the sketch it is possible to notice how the two angles present a non-linear relationship: in case that α overcomes 40°, β rapidly reaches values higher than 90°.

After trying to solve the problem using different numerical approaches, a polynomial regression has been chosen as the best way to relate the two angles.

A set of related angles has been considered and as a polynomial degree, a 4th-degree polynomial showed the best results: the polynomial form that suited the regression can be seen in Equation (3). Following, the regression data, particularly consultable in Table 3 and Table 4:

$$\beta = 1.5(10^{-5})\alpha^4 - 1.3(10^{-4})\alpha^3 - 7.5(10^{-2})\alpha^2 + 4.6(10^{0})\alpha - 4.5(10^{-1}) \quad (3)$$

$$r^2 = 0.999$$

$$r_{adj}{}^2 = 0.999$$

The residual standard error resulted in 0.069 in 9 degrees of freedom.

Table 3 Polynomial coefficients

Coefficient	**Estimate**	**Standard Error**	**t-statistic**	**p-value**
β0	-0.451	0.117	-3.849	0.004
β1	4.600	0.051	90.562	0.000

β2	-0.075	0.006	-11.985	0.000
β3	0.000	0.000	-0.464	0.654
β4	0.000	0.000	3.537	0.006

Table 4 Regression data

Source	**df (Degrees of Freedom)**	**SS (Sum of Squares)**	**MS (Mean of Squares)**	**F-statistic**	**p-value**
Regression	4	6591.591	1647.898	349277.780	0
Residual Error	9	0.042	0.005	-	-
Total	13	6591.633	507.049	-	-

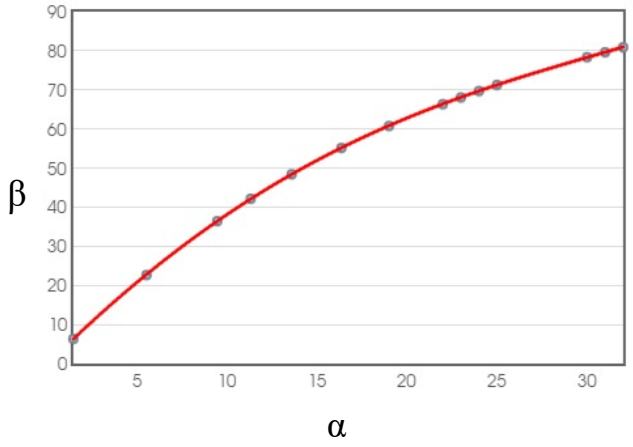

Figure 22 α-β

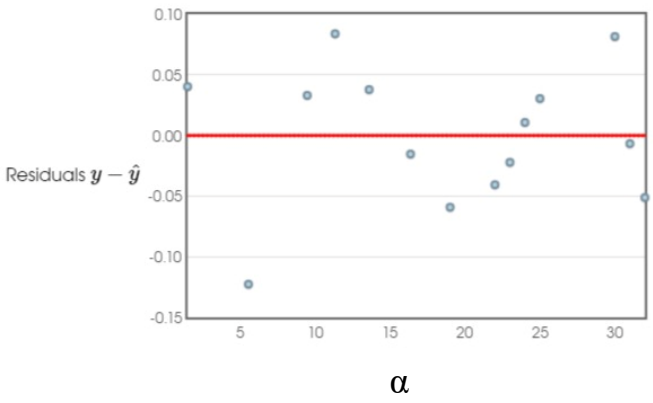

Figure 23 α-β Residuals

Looking at the outcomes (Table 3 and Table 4, Figure 22 and Figure 23) and correlating the polynomial form with experimental data, the approximation has been evaluated as very accurate, hence the angles could be considered through this relationship.

The components requiring their manufacturing would be so:

- Driver pulley (Additive Manufacturing);
- Swinging arm (CNC machining and laser cutting);
- Potentiometer bracket (Structural Steel);
- Bracket (Laser cutting and cold press-bending).

4 Setup Realization

Having decided the type of assembly to be produced, different manufacturing processes were chosen.

Indeed, the main processes that were employed in the making of the components were:

- CNC machining on steel parts (brackets and swinging arm);
- Lathe operations (rod);
- Additive manufacturing (supports and mounts).

4.1 Steering Column Mounts

The driver pulley, since a beltless design was chosen, underwent some design changes. Indeed, losing the purpose of transmitting the motion by means of a belt, the internal groove was completely removed, leaving only the circular external surface extruded as a single unit.

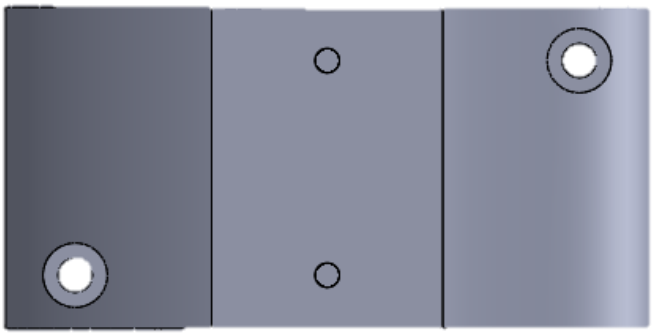

Figure 24 Front view of the mounting

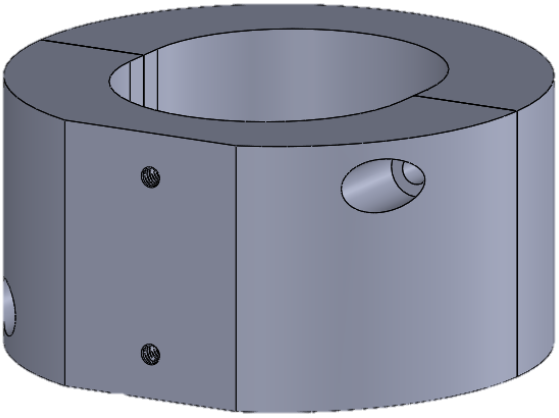

Figure 25 Isometric view of the mounting

The two different components creating the mounting assembly were manufactured by 3D-printing them. The material chosen for the extrusion is the largely used PLA.

The threads featured in CAD software were parametrized in G-Code (Code used by 3D-printers) and were implemented in the printing process. Even if at first a lot of concerns rose about this,

the final product successfully came out as robust. In fact, no secondary threading was necessary, being the feature already robust and fully functional (notice that the threads under test were M3 ones).

4.2 New Potentiometer

In contrast with the original design choices, the potentiometer mounted on the setup is no more a multi-turn one. Having a single turn potentiometer, referring to the same applied voltage, permits to obtain a better resolution in the subsequent readings.

Being it a single turn potentiometer means that in 270° its resistance can change from 0 Ω to its max value, 100 kΩ.

Since the available steering range is set to 120°, only a portion of the resistance range can be employed. Indeed, the first and last 75° of rotation result unusable due to the steering limits of the e-scooter.

The chosen potentiometer is defined as a 100 kΩ variable resistor, so, thanks to the linearity of its characteristics, it is calculated the effective range of resistance that can be provided. At first, a useful information is how many ohms per degree of rotation are

changing. Based on Table 5, the first relation to be found is expressed in Equation (4).

Table 5 Electrical circuit parameters

Parameter	Meaning
R_{max}	Potentiometer resistance rating [kΩ]
φ_{max}	Maximum angular range [°]
R_{φ}	Resistance per angle of turning [Ω/°]
R_L (R_R)	Resistance found at maximum anticlockwise turning (clockwise) [Ω]
φ_L (φ_R)	Angle at maximum anticlockwise turning (clockwise) [°]

$$\frac{R_{max}}{\varphi_{max}} = R_{\varphi} = \frac{100\ \text{k}\Omega}{270°} = 370.370\,\frac{\Omega}{°} \quad (4)$$

In its most anti-clockwise position, the resistance of the potentiometer, intended as the initial one, is expressed in Equation (5).

$$R_L = R_{\varphi}\varphi_L = \left(370.370\,\frac{\Omega}{°}\right)(75°) = 27.778\ \text{k}\Omega \quad (5)$$

By contrast, in its most clockwise position the resistance can be found as in Equation (6).

$$R_R = R_\varphi \varphi_R = \left(370.370 \frac{\Omega}{°}\right)(195°) = 72.222\ \text{k}\Omega \quad (6)$$

Having defined this range, it is possible to evaluate the voltage read by the SCADAS by simply solving the voltage partition according to the following circuit, Figure 26:

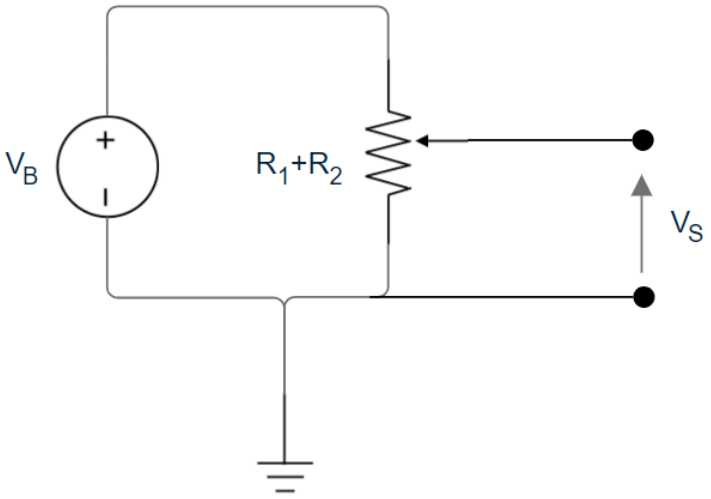

Figure 26 Potentiometer electrical circuit

Since the employed potentiometer is a linear characteristic one, its representation can be made by a linear characteristic variable resistor. As simple as it seems, the voltage partition rule deals with such a component like it would with two different resistors in series, changing their value accordingly to the cursor

position. In the next figure, Figure 27, the simplification can be hence appreciated.

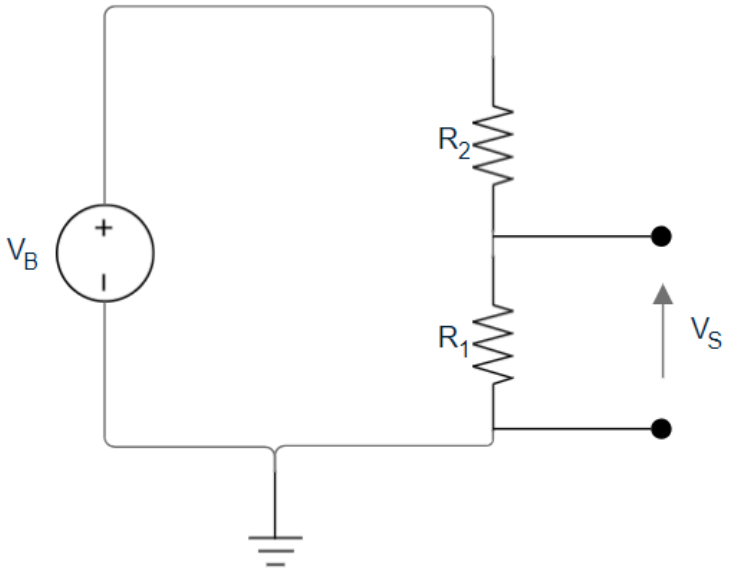

Figure 27 Potentiometer equivalent electrical circuit

Considering the battery voltage to be nominally 7.4 V, the SCADAS reading can oscillate between two extreme values defined by the two extreme values of the resistance of the potentiometer. However, it must be taken into account that this parameter is reliant on the State of Charge (SOC) and the loading conditions of the battery. Following the best-practice approach, the battery voltage should be also monitored in order to match the real relationship between the readings and the angle of the potentiometer shaft.

Coming back to the limit values calculation, the two extreme values will be evaluated following the previously results. With the subscript 'L' will be indicated the maximum left steering angle, with the subscript 'R' will be instead indicated the opposite turn angle.

In order to correlate the variable resistance to the read voltage, according to (7)

Table 6, it is useful to define the partition factor as in the Equation (7).

$$\gamma = \frac{R_1}{R_1 + R_2}$$

(7)

Table 6 Equivalent resistance parameters

Resistance	**Range**
R_1	0÷100 kΩ (R_1=100-x)
R_2	100÷0 kΩ (R_2=x)

Defined this parameter, the relation between output/input voltages can be written as this linear equation, Equation (8):

$$V_S = \gamma V_B$$

(8)

The voltage that can be read by the SCADAS is so a quantity that depends on the partition factor and the voltage applied to circuit.

Being the potentiometer directly connected to the battery, neglecting the wires and connections impedance, the source voltage only changes in case of varying SOC or strongly changing loading conditions (very improbable). Said so, the discriminant actor is the cursor position, dictating the partitioning factor. This means that, as intended, the read voltage is 1:1 related to the position of the steering column through the position of the cursor present in the linear potentiometer.

Referring to previously calculated limit resistances, the corresponding limit partition factors and limit read voltages are deducted.

$$\gamma_L = \frac{R_1}{R_1 + R_2} = \frac{27778\ \Omega}{27778\ \Omega + (100000\ \Omega - 27778\ \Omega)} = 0.278$$

(9)

$$V_{S,L} = \gamma_L V_B = 0.278\ (7.4\ V) = 2.056\ V$$

(10)

$$\gamma_R = \frac{R_1}{R_1 + R_2} = \frac{72222\ \Omega}{27778\ \Omega + (100000\ \Omega - 27778\ \Omega)} = 0.722$$

(11)

$$V_{S,R} = \gamma_R V_B = 0.722\ (7.4\ V) = 5.344\ V$$

(12)

Table 7 Partition parameters

Parameter	Meaning
V_S	Available supply voltage, here corresponding to V_B [V]
V_B	Available resolution [mV/°]
γ	Partition factor [-]
γ_L (γ_R)	Angle found in maximum left (right) steering [°]
$V_{S,L}$ $(V_{S,R})$	Voltage read in maximum left (right) steering [V]

To have a quick check, it is also possible to derive the same results considering the overall voltage span across the useful angular range as in Equation (13) (now following Table 8 values).

$$\frac{V_{av}}{\varphi} = V_{\varphi}$$

(13)

$$\frac{7400\ mV}{270°} = 27.407\frac{mV}{°}$$

(14)

$$V_L = \varphi_L V_{\varphi} = (75°)\left(27.407\frac{mV}{°}\right) = 2.056\ V$$

(15)

$$V_R = \varphi_R V_\varphi = (75° + 120°)\left(27.407\frac{mV}{°}\right) = 5.344\,V$$

(16)

A quick overview of the employed parameters found in the analysis can be found in Table 8.

Table 8 Partition parameters 2

Parameter	Meaning
V_{av}	Available supply voltage, here corresponding to V_B [V]
φ	Angular range of the potentiometer [°]
V_φ	Available resolution [mV/°]
V_L (V_R)	Voltage read in maximum left (right) steering [V]
φ_L (φ_R)	Angle found in maximum left (right) steering [°]

In both cases, over the span of 120° permitted by the steering column, a range of 3.288 V is obtained. This voltage range, considering the $27.407\frac{mV}{°}$ resolution, is more than enough to well estimate and correlate the steering angle.

4.3 Metal Components

All the metal components like the brackets, the rod and the swinging arm were manufactured in structural steel.

For what concerns the brackets and swinging arm, laser cutting and a refine at the mill machine were the two processes that perfectly suited the needs. The laser cutting was delegated to a professional shop while the millings were performed by the author.

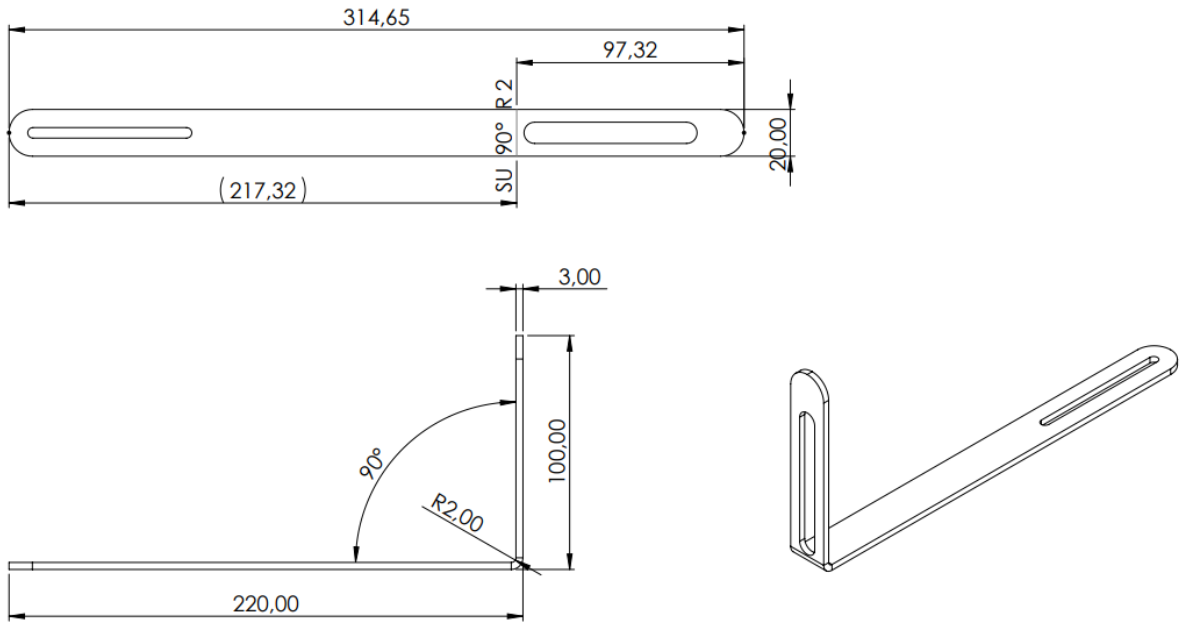

Figure 28 Bracket

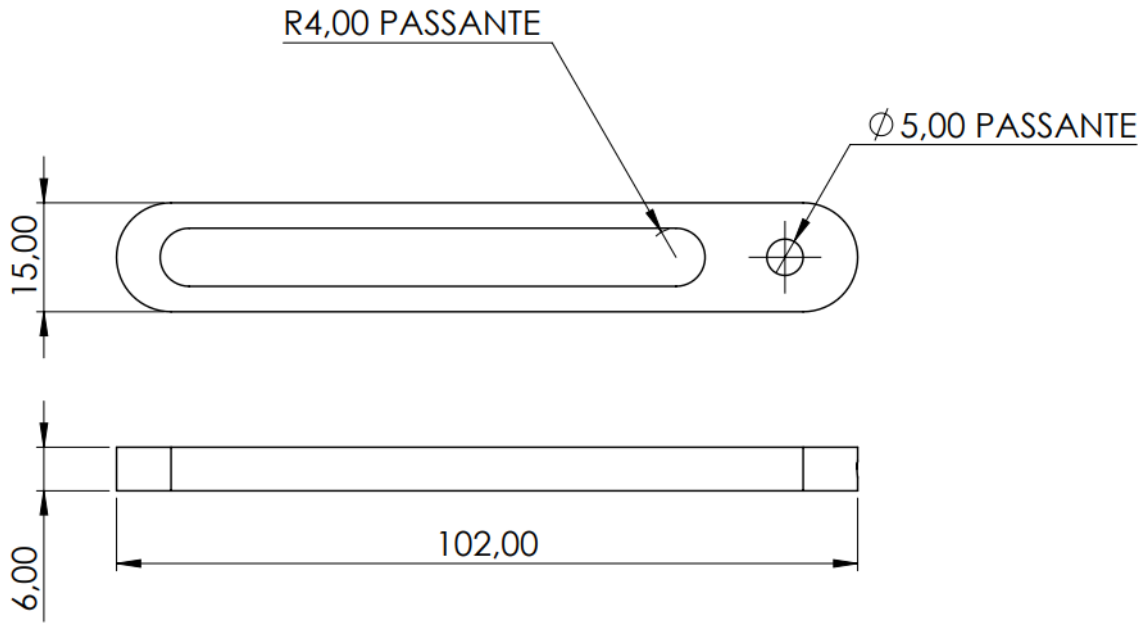

Figure 29 Driven arm

Looking at Figure 28 and Figure 29 it is possible to see the drawings that were sent to the shop in order to generate the G-code employed by the laser cutters.

The additional millings were needed to finish the surfaces and to smoothen out radii and sharp corners. Also, threaded hole was performed on the driven arm side to accomodate a screw locking the potentiometer shaft in place.

Instead, the rod was turned on a metal lathe, following the dimensioning present in Figure 31. Notice that two designs were considered (Figure 30 and Figure 31), and both were built; however, only the latter was then used.

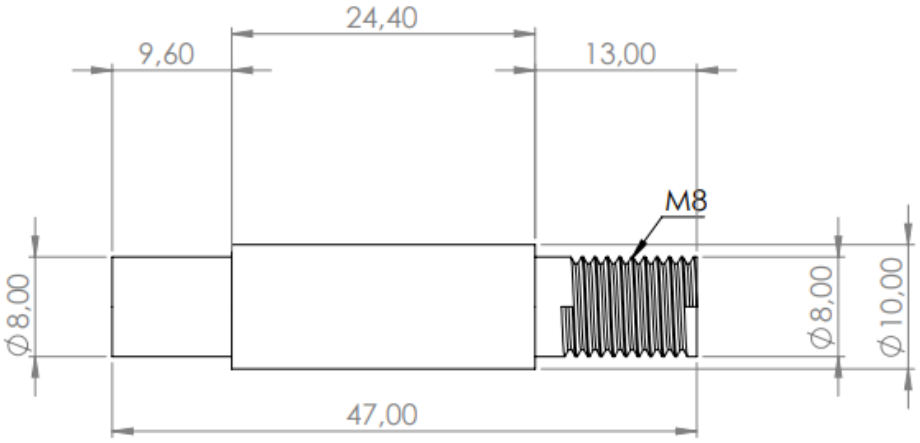

Figure 30 Rod first sketch

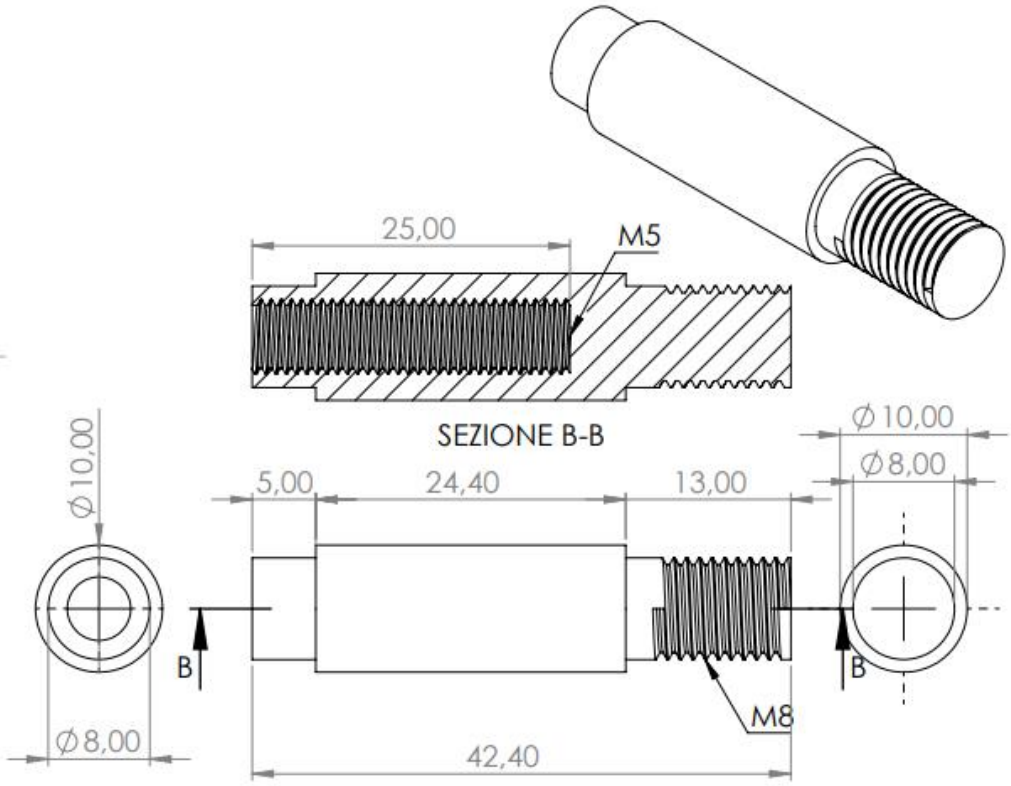

Figure 31 Rod definitive sketch

4.4 PLA

Talking about the additional manufactured components, the material to be chosen was the first issue to solve.

The PLA is the best take in the additive manufacturing of such parts. The filament that has been used to print the parts of the proposed setup presents the following characteristics [12]:

- Nominal diameter: 2.85 mm ± 0.10 mm
- Max circular deviation: 0.10 mm
- Net weight: 350 g / 44 m

The material presented the suitable mechanical properties (Table 9) to achieve the required results:

Table 9 PLA properties

Property	Value	Test
Tensile modulus	2346.5 MPa	ISO 527 - 1 mm/min
Yielding strength	49.5 MPa	ISO 527 - 50 mm/min
Yielding elongation	3.3%	ISO 527 – 50 mm/min
Flex modulus	103.0 MPa	ISO 178
Impact resistance	5.1 kJ/m^2	ISO 178
MFR	0.609 g/min	ISO 1133 – 210°C 2.16 kg

In order to use the filament in the 3D-printing process, an extruder of 0.4 mm in diameter heated up to 210°C was used. The printer used to fulfil the manufacturing is an Ultimaker 3 Extended.

The parts were printed using the parameters in Table 10:

Table 10 Printing parameters

Parameter	**Value**
Layer height	0.25 mm
Infill density	50 %
Infill pattern	Cross
Printing temperature	205°C
Building plate temperature	60°C
Print speed	45 mm/s

To accomplish the final results, numerous prints were discarded, and a lot of misprints were made. The problem that were arising were all related to the printers, so after some troubleshooting and tuning all the components were correctly printed.

4.5 Mounting

In order to fix all the components together, the right fastening method must be taken into consideration: in this particular case, threaded fasteners seemed the best take.

By checking the design and the CAD models, it was found that a total of 6 M3 screws is required. Following the constraints given by the assembly, the dimensions were taken and used to create the suitable Bill of Materials.

4.5.1 Fasteners

Following in Table 11 and Figure 32, the dimensions picked for the threaded fasteners:

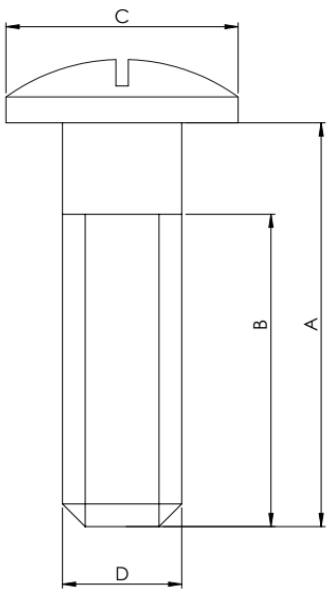

Figure 32 Screw parameters

Table 11 Fasteners dimensioning

	Interface		
Dimension	**Upper mounts**	**Upper mounts/Upper bracket**	**Bottom bracket/Deck**
A_{MAX}	21.17 mm	14.64 mm	16.5 mm
A_{MIN}	15 mm	12 mm	12 mm
B	10 mm	12 mm	10 mm
C	5.5 mm – 6 mm		
D	M3 x 0.5 mm		

For each fastening, a number of two M3 screws is required. As a choice, the length of each screw is trimmed to dimension: the upper-mounts screws are trimmed to 15 mm, the upper-interface screws to 12 mm and the bottom-interface screws to 15 mm.

These fastening components allow to get the proper possibility to align and accommodate the various components without worrying about losing contact between male and female threads.

5 Acquisition System

Core of the experimental setup is the acquisition system, the ensemble of sensors and processing units used to retrieve the data in the manoeuvring of the e-scooter. For the purpose of any dynamics study, the acquisition system must be able to measure and collect:

- The cartesian accelerations of the e-scooter (x, y and z directions),
- The cartesian accelerations of the driver (x, y and z directions),
- The steering angle,
- The wheels angular velocities.

5.1 Siemens SCADAS XS

The SCADAS XS provided by Siemens (Figure 33) is the heart of the acquisition system: through a multitude of ports, it acquires the different signals and it is able to collect and perform a preliminary processing of the data.

It comes with 4 analogue ports called LEMO-ports, two ports connectable to the two tachometers, a GNSS-port for a GPS antenna and a CAN port.

Figure 33 SCADAS XS

5.2 SBG-Inertial Sensor

A MEMS-sensor, it is made by three individual sub-sensors:

- A triaxial gyroscopic sensor,
- A triaxial accelerometer,
- A triaxial magnetometer.

To better suite the collected data to the real-world application, it must be placed as close as possible to the COG of the vehicle (Figure 34).

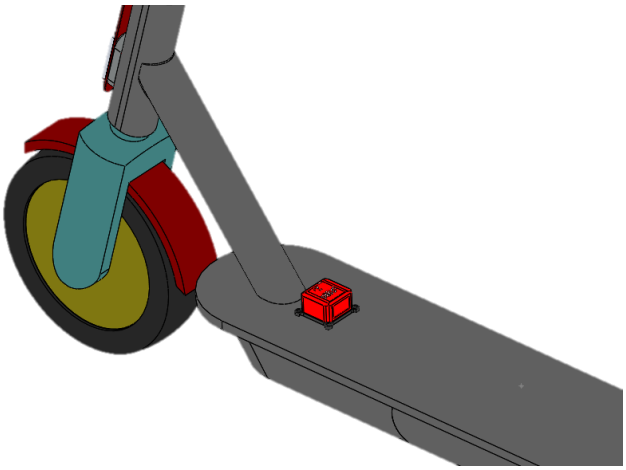

Figure 34 SBG positioning

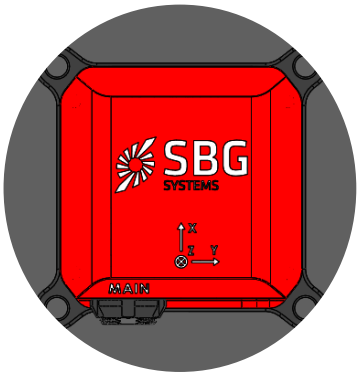

Figure 35 SBG

5.3 Tachometers

A pair of Gebildet LJ12A3-4-Z proximity sensors is employed, sampled at 200 Hz.

The first of the two sensors is mounted on the front wheel of the vehicle, where the e-motor is installed. On the wheel rim, a

circular repetitions of 6 equally spaced screws is mounted (Figure 36).

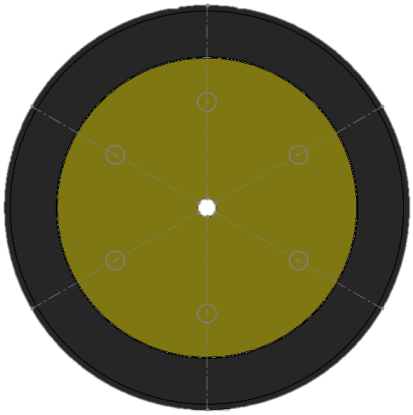

Figure 36 Front wheel

At each wheel rotation, every screw passage is captured by the proximity sensor mounted on the frame. By relating the number of acquired pulses to the time-steps, the angular velocity is evaluated.

For what concerns the rear wheel, the same procedure is applied. However, already having 5 spokes on the wheel, the screws can already be mounted on such features (Figure 37).

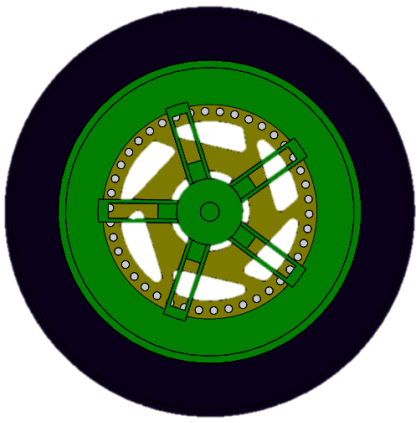

Figure 37 Rear wheel

5.4 Opal APDM

An inertial system used to retrieve the inertial parameters of the driver. A common Access Point collects the data of 5 different wireless wearable MEMS units.

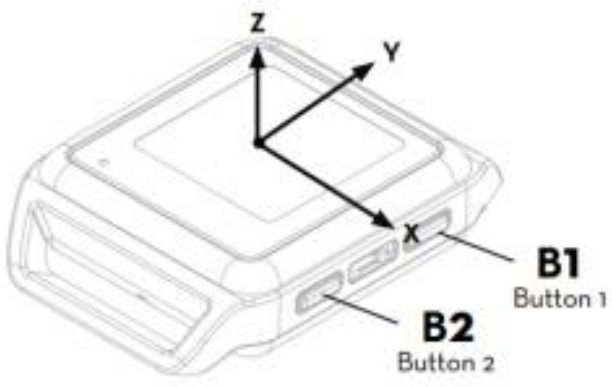

Figure 38 Opal wearable

5.5 Steering Angle

The steering angle is measured as previously explained, through the reading of the variation of resistance of an angular potentiometer, linked to the steering column through a mechanical linkage system.

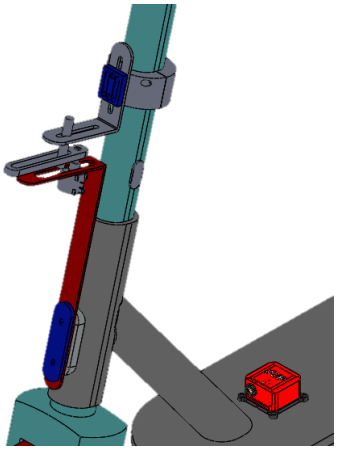

Figure 39 Steering angle measuring system

5.6 Battery

Since most of the employed systems are active ones, the eletric supply is provided by a 7.4 V LiPo battery.

Figure 40 LiPo Battery

6 Analytical Relationships

The mathematical relationship between the two angles is very straightforward if the system is considered at a determined time instant. Indeed, the equation relating the two features is a simple trigonometric function.

6.1 Relevant Parameters

Following in Table 12, the nomenclature:

Table 12 Parameters

Parameter	Description
R	Distance between steering axis and rod axis (i.e., the radius of the trace made by the rod)
r	Distance between the potentiometer shaft axis and the rod axis
α	Angle between R and the longitudinal axis
β	Angle between r and the longitudinal axis

6.2 Analytical Formulation

The analytical form is expressed in Equation (17):

$$R \sin \alpha = r \sin \beta \tag{17}$$

Sketching the geometrical representation, the system is depicted as the Figure 41 suggests.

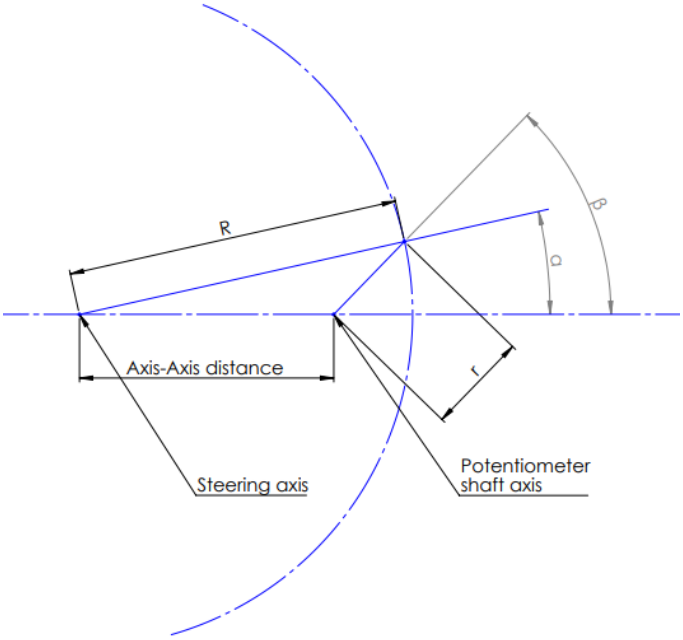

Figure 41 Geometrial/Kinematic sketch

By setting an arbitrary angle (it is the same if α or β is chosen), the trigonometric equation can be verified.

In the current setup, the parameters are defined as in Table 13.

Table 13 IRL Parameters

Parameter	Value
R	83 mm
r	34.85 mm (dictated by the angles)
α	22.89 ° (derived by the mathematical relation)
β	67.92 ° (randomly chosen)
Axis – Axis distance	63.36 mm

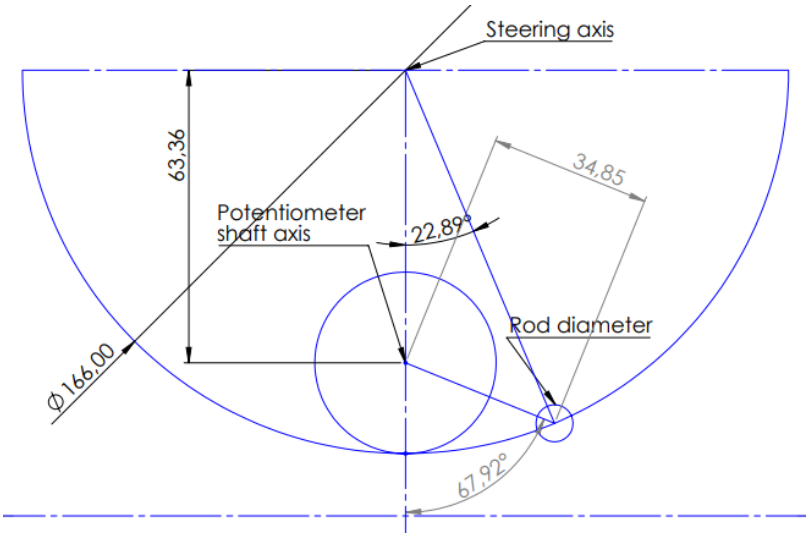

Figure 42 Geometrical sketch

By applying the above relationship, knowing all except the steering angle:

$$\frac{166}{2}\sin\alpha = 34.85\sin 67.92°$$

(18)

$$\sin\alpha = \frac{2}{166}34.85\sin 67.92°$$

(19)

$$\alpha = \sin^{-1}(\frac{2}{166}34.85\sin 67.92°) = 22.89°$$

(20)

It is shown that such relationship fulfils the demands (following Figure 42).

6.3 Sliding Rod Issue

However, the problem of making up an universal solution is represented by the non-constant parameter ‘r’, that changes according to the steering angle. This is due to the fact that the rod can slide in the buttonhole, changing the distance of the rod axis with respect to the potentiometer shaft one.

Anyway, the consistency of the abovementioned equation still holds as long as the ‘r’ parameter is changed accordingly.

As a verification, from Figure 42 a different angle is chosen, and what results can be seen in Figure 43, accordingly to Table 14.

Table 14 IRL Parameters, different angle

Parameter	**Value**
R	83 mm
r	25.31 mm (dictated by the angles)
α	12.64 ° (derived by the mathematical relation)
β	45.84 ° (randomly chosen)
Axis – Axis distance	63.36 mm

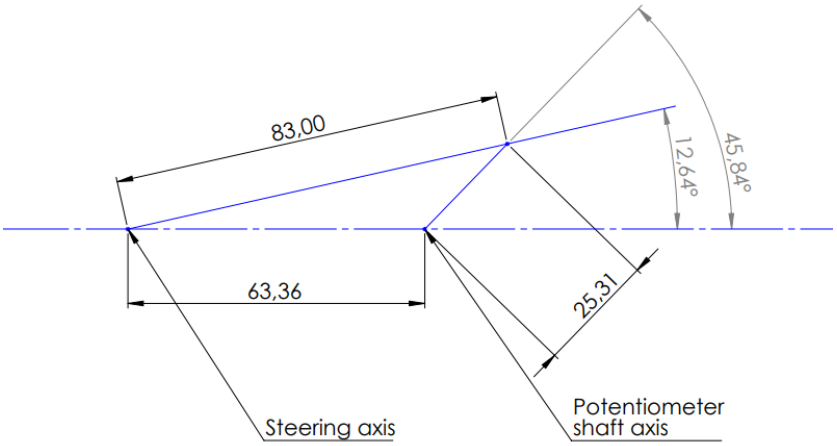

Figure 43 Geometrical sketch, different angle

$$\frac{166}{2}\sin\alpha = 25.31\sin 45.84°$$

(21)

$$\sin\alpha = \frac{2}{166}25.31\sin 45.84°$$

(22)

$$\alpha = \sin^{-1}(\frac{2}{166}25.31\sin 45.84°) = 12.64°$$

(23)

Being this the problem, the solution has been found in linearly approximate the relationship (refer to 3.8).

6.4 Kinematics

To better understand the kinematics of the system and the application of such a formulation, a useful representation can be found in the mechanical visualization of the system, as can be seen in Figure 44.

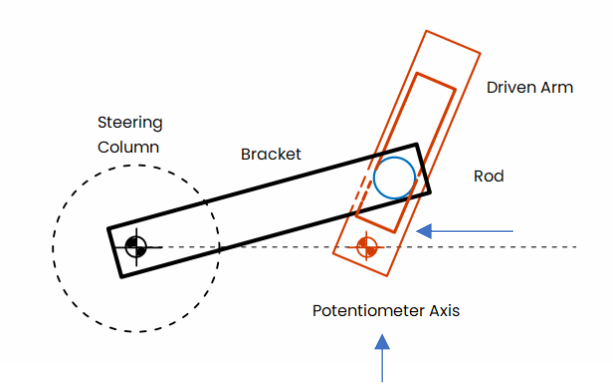

Figure 44 Mechanical representation

In Figure 44, it is depicted the system as seen from the top. Applying the same nomenclature as before (Table 13), the system can be reduced to Figure 45.

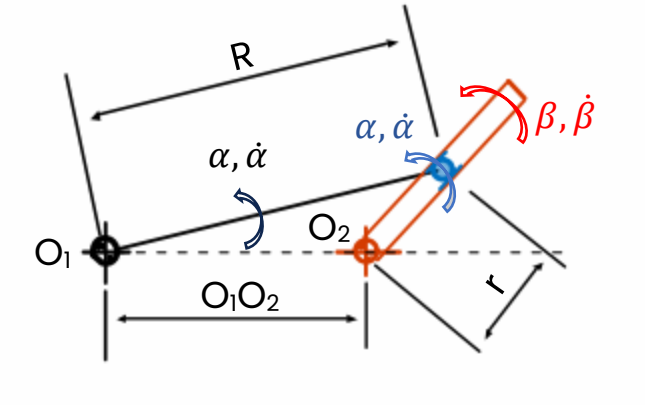

Figure 45 Mechanical representation, DOFs

Where O1 and O2 respectively refer to the steering axis and the potentiometer shaft axis, while the point A refers to the rod axis.

In Figure 45, the DOF of the linkages can be appreciated, being them shown also in Table 15:

Table 15 DOFs

α	Steering angle
$\dot{\alpha}$	Steering angular velocity
β	Potentiometer shaft angle
$\dot{\beta}$	Potentiometer shaft angle velocity

Particularly, the joints and hinge types can be seen:

- The bracket is fixed, and its only possible movement is a rotation around the O1 axis;
- The rod is fixed to the bracket and moves accordingly to the steering angle while a prismatic joint transmits its motion to the driven arm;
- The driven arm is hinged like the bracket but it is pulled by the prismatic joint interfacing itself with the rod element.

7 Preliminary Testing

Although the study is devoted to the design and realization of a steering angle measuring system to have a better understanding of the lateral dynamics of an e-scooter, a preliminary experimental analysis is performed on a longitudinal dynamic manoeuvring.

A total of 9 tests were conducted, each one studying a particular case of braking in a Xiaomi Pro 2 e-scooter (Table 16):

Table 16 Test description

Test 1, Test 2	Light braking
Test 3, Test 4	Intermediate-intensity braking
Test 5, Test 6	Hard braking
Test 7	Light braking, redundant test
Test 8	Intermediate-intensity braking, redundant test
Test 9	Hard braking, redundant test

The signals were acquired through two different acquisition systems, being Opal and Scadas. Due to this duality of instrumentation, a trigger signal was necessary to match the time scale of the different sensors.

7.1 Matlab Environment

What was retrieved was then rearranged in a MATLAB file with *.mat* extension. This file is made up of 18 different structs, by using as nomenclature *Signal_0i*, being *i* an increasing variable from 0 up to 9, *Signal_1j* being *j* an increasing variable from 0 up to 7.

Each struct is made by 3 additional sub-structs:

- x_values;
- y_values;
- function_record.

In every sub-struct, all the information about the signal are stored: eventual offsets, refactoring constants, time steps and so on.However, in order to be processed, the signals corresponding to the 18 main structs must be recognized: by studying the multiple data, the nomenclature folds as follow:

Table 17 Signals nomenclature

Signal_00	Trigger signal
Signal_01	Front tachometer, raw
Signal_02	Front tachometer
Signal_03	Rear tachometer, raw
Signal_04	Front tachometer
Signal_05	Euler yaw
Signal_06	Euler pitch

Signal_07	Euler roll
Signal_08	*First quaternion*
Signal_09	*Second quaternion*
Signal_10	*Third quaternion*
Signal_11	*Fourth quaternion*
Signal_12	Gyroscopic Z
Signal_13	Gyroscopic Y
Signal_14	Gyroscopic X
Signal_15	Vertical acceleration (Z)
Signal_16	Lateral acceleration (Y)
Signal_17	Longitudinal acceleration (X)

Notice that some elements (i.e., quaternions) in Table 17 are written in italic: this is due to their lack of relevance in the present document, hence not too many details will be provided.

As for this report, all the considerations are made considering the first test. All the processing is the same for all the acquisitions, except for the name of the data file that need to be loaded in the multipurpose script.

7.1.1 Tachometer's Signals Duality

At a first glance, it is immediately noticed the double signal referred to both the tachometers. To investigate the nature of this feature, the first signal to be studied is the *Signal_01* (the same concepts can be applied to its counterpart, *Signal_03*).

Once the signals are collected, a for-loop can be employed to reiteratively fill a blank array with the information contained in the studied struct. Following the nomenclature of the struct (Table 17), an x-values array and a y-values one are created.

Plotting the two arrays results in a timescale function of an unitarily increasing x-axis: the hypothesis is that such a set of data could be representing the number of pulses transmitted by the sensor.

Following this hypothesis, the 'x' and 'y' values are plotted by switching their axis order.

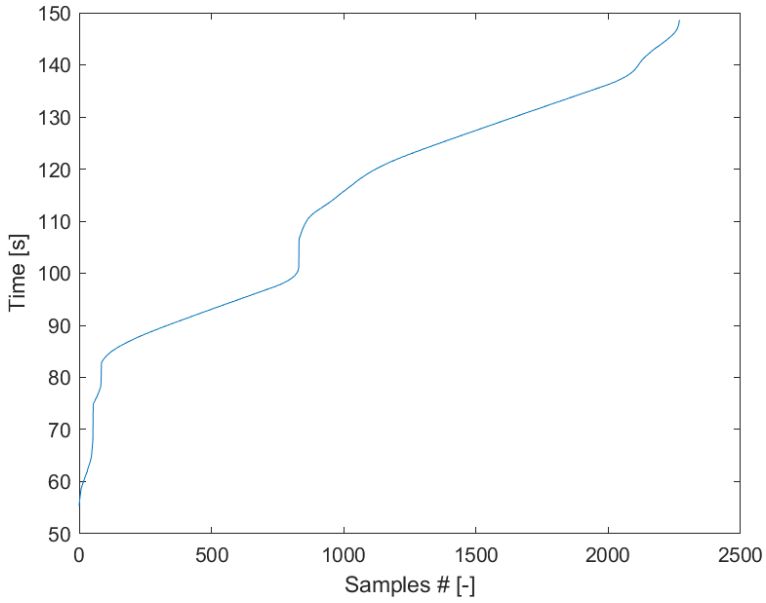

Figure 46 Raw signal

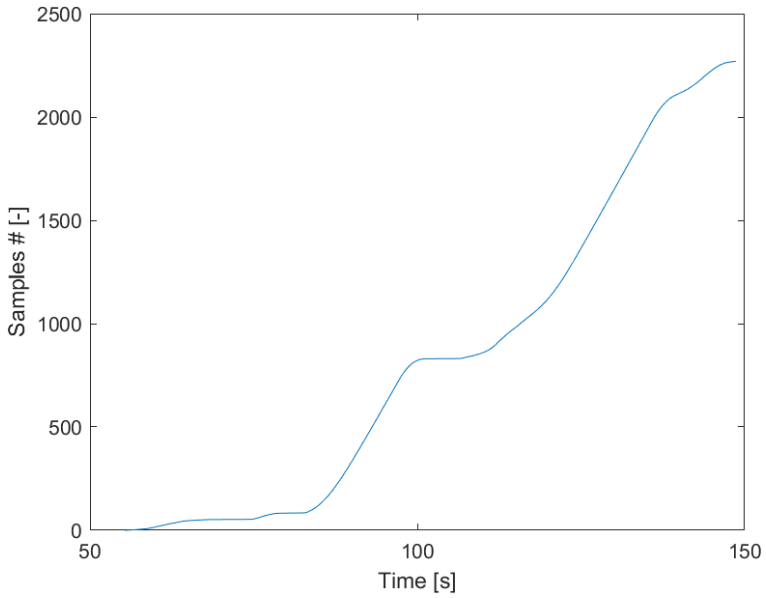

Figure 47 Raw signal, inverted axis

By looking at the second, inverted, plot in Figure 47, the increasing trend seems to confirm the initial hypothesis.

Since the previously called 'y_1' is displaying time, a change of variable is made, restoring the correct data-dictionary.

Considering then that 6 pulses correspond to a full rotation of the front wheel (5 in the case of the rear one), its rotational velocity can be calculated by differentiating the time array. In fact, the signal contains the number of pulses read in a time range.

In order to keep consistency between arrays dimension, due to the losing of a cell by means of differentiating, the last value of omega must be written "by hand".

To finally verify the hypothesis, the newly calculated quantities can be plotted. Moreover, the radius of the wheel in meters is taken into account to retrieve the speed information in m/s, while a conversion factor is used to switch between rad/s and rpm units. Such a conversion factor is obtained simply from Equation (24), where the unit conversion takes place.

$$[rpm] = \frac{60\left[\frac{rad}{s}\right]}{2\pi} = 9.549[\frac{rad}{s}] \qquad (24)$$

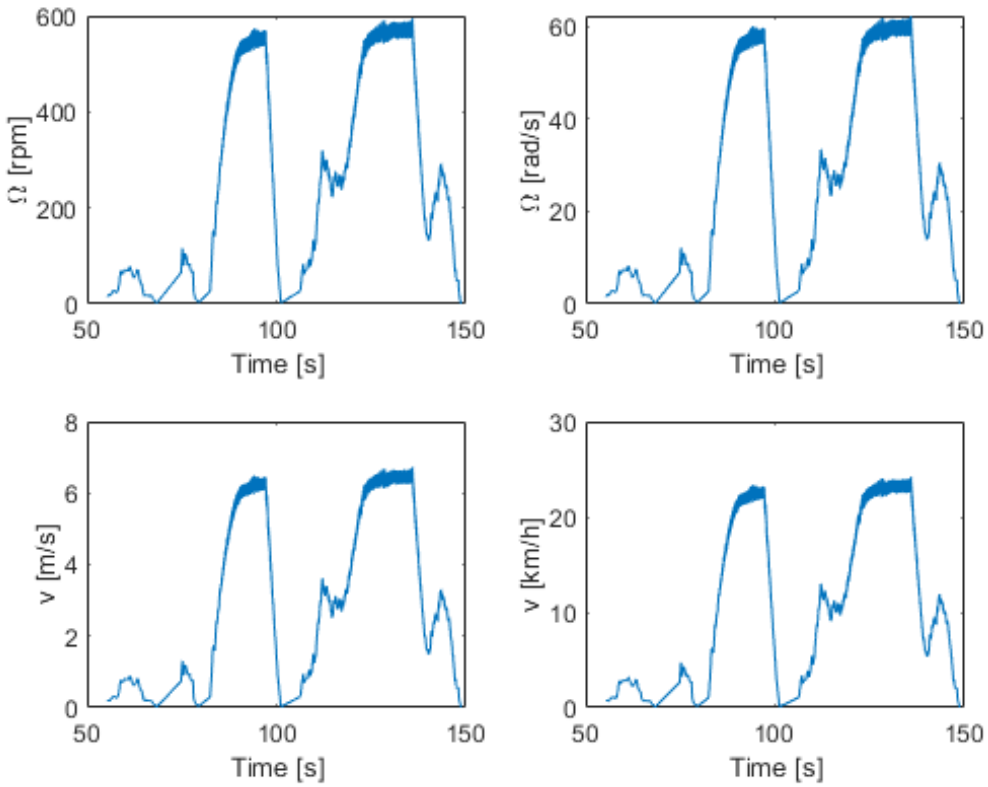

Figure 48 Post-processed raw signal

To see and univocally verify the processing, a comparison between the final raw signal and the pre-processed signal can be put in place as can be seen in Figure 49.

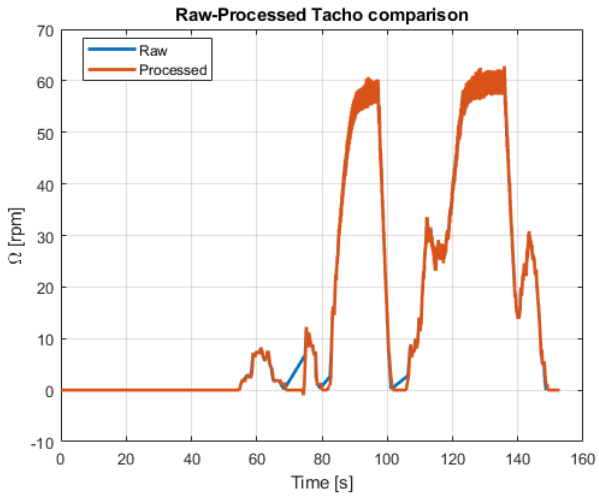

Figure 49 Raw/Processed signals comparison

As Figure 49 shows, the two signals match perfectly, except for those points where the vehicle started, hence where no pulses were yet transmitted. Due to the nature of the differentiation, these points appear to interpolate the 0-velocity to a non-null value in proximity of the starts. Apart from this analytical trifle (a better view is proposed in Figure 50), the two signals can be considered identical.

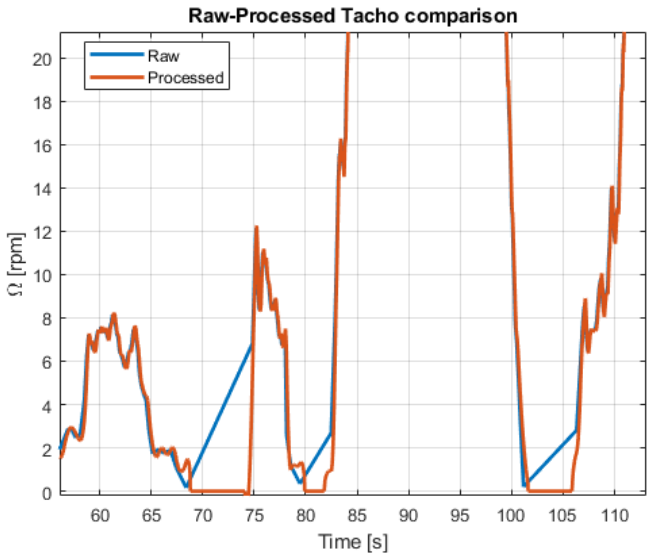

Figure 50 Raw/Processed detail

Having this hypothesis verified, it is possible to move on to the study of the entirety of the signals.

7.1.2 Processing

As a first step, a struct containing all the signals is built.

Then, before entering in the main loop (used to study all the signals in the same script), a struct defining the angular velocities is built.

After having defined the omega-struct (where velocities and time are related), the main loop can start: it is iterated from 1 (since 1 is the minimum index MATLAB can process) to the last signal. In the first portion of the loop, a series of preliminary

checks is performed, where the test information are saved and eventually displayed.

A time vector must be defined for the signals, hence an additional inner loop is employed, where through an iterative summation of timesteps an array is built.

At this point, to properly manage the arrays, the signal name information must be retrieved. However, it was noticed that the string corresponding to the name presented '_' characters; to prevent the software reading these as Latex entries, a small for-loop was introduced to substitute these characters with blank spaces.

Building a struct that iteratively increase in size such as *Name(count1).name* permits to maintain the data sorted even if out of the corresponding loop.

Next, a condition has to be made: if the iteration encounters one of the raw signals, the abovementioned processing must be performed (the case of Figure 46 and Figure 47). Moreover, to fill the proper struct entries, a switch function must be used, distinguishing the front by the rear sensor signal.

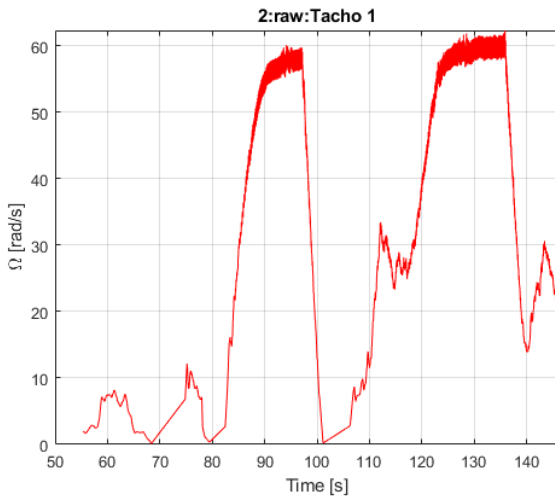

Figure 51 Raw signal, front

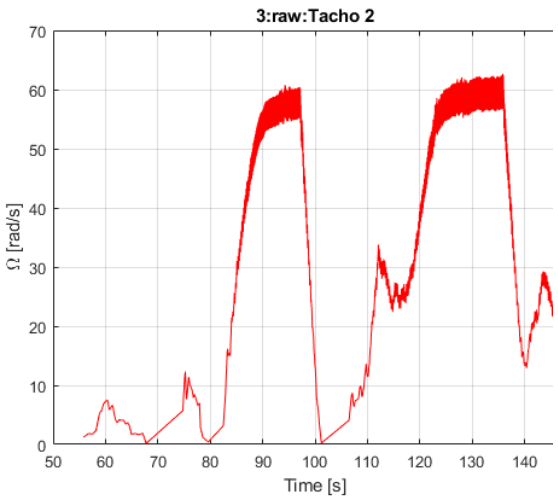

Figure 52 Raw signal, rear

If none of the raw signals is encountered, the script follows, managing the entries and creating plots and figures.

Also here, a switch function is used to assign the proper labelling to the signals. This switch function is mandatory to properly assign the correct units and the correct layout to the right quantities.

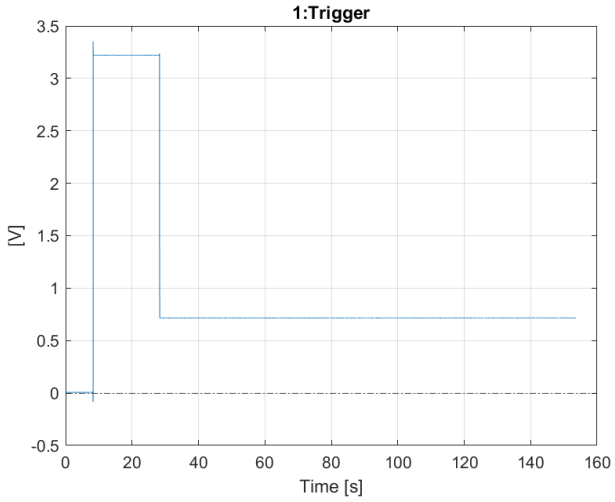

Figure 53 Trigger signal

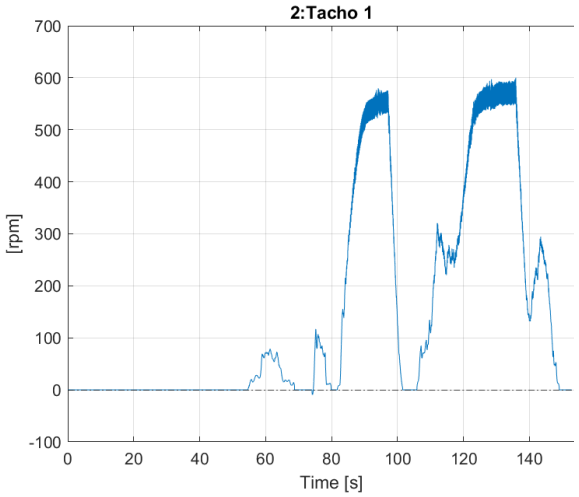

Figure 54 Front tachometer

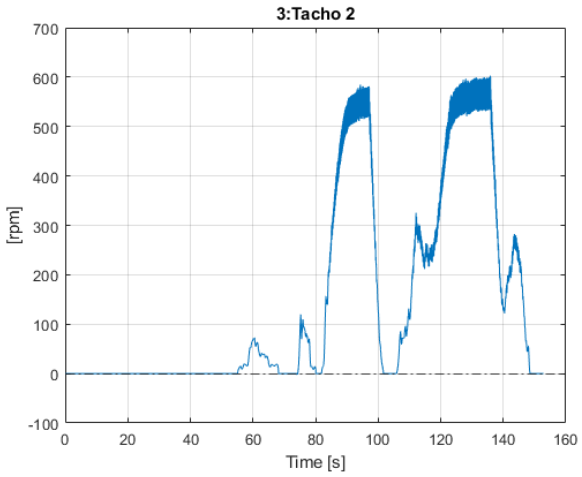

Figure 55 Rear tachometer

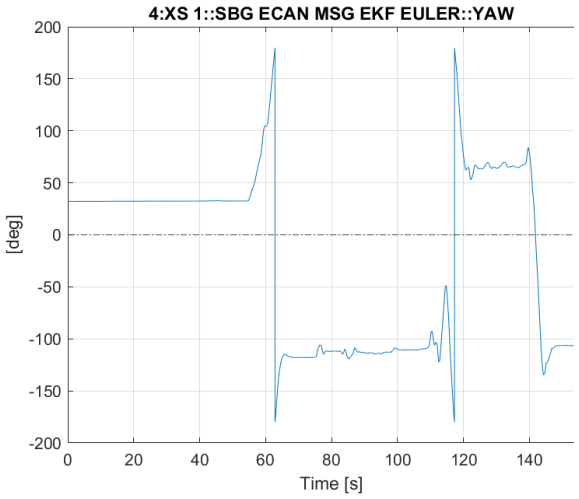

Figure 56 Yaw signal

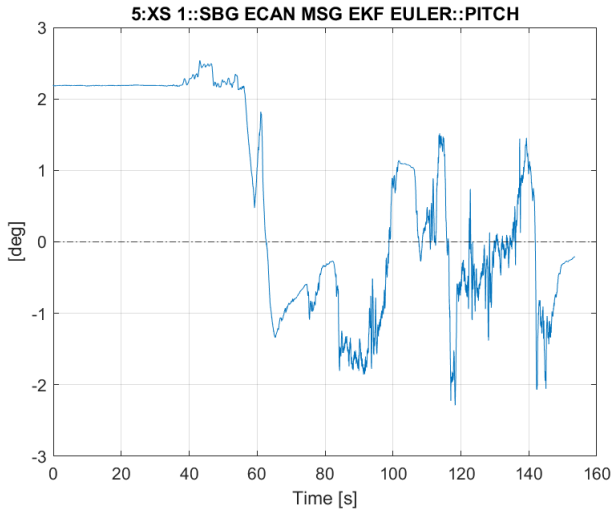

Figure 57 Pitch signal

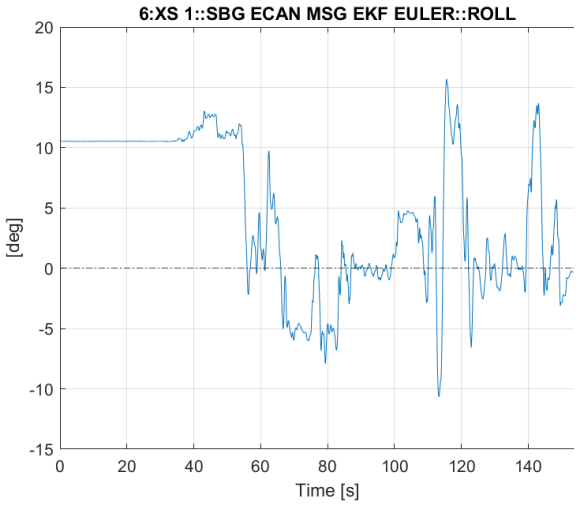

Figure 58 Roll signal

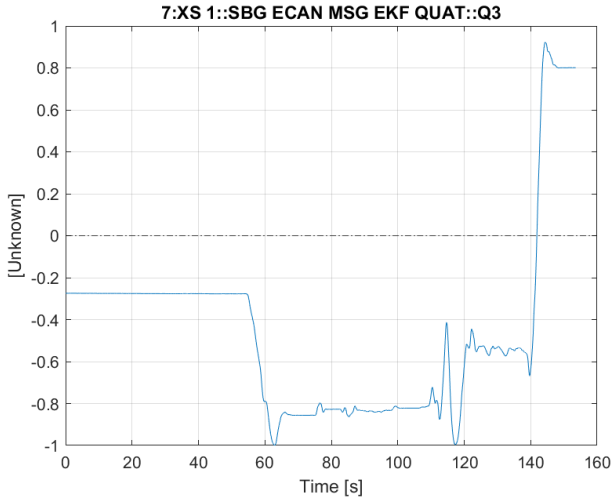

Figure 59 Quaternion 3

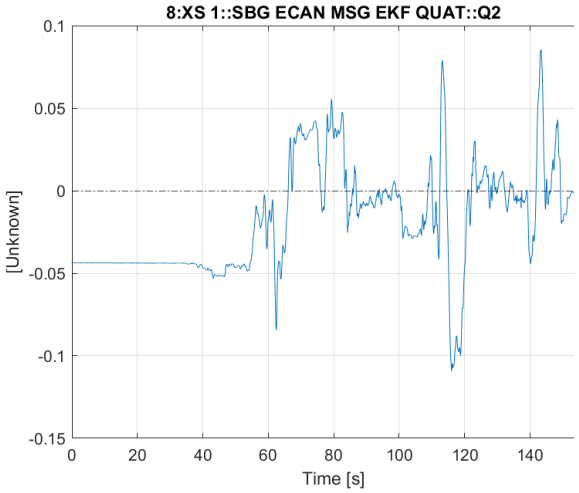

Figure 60 Quaternion 2

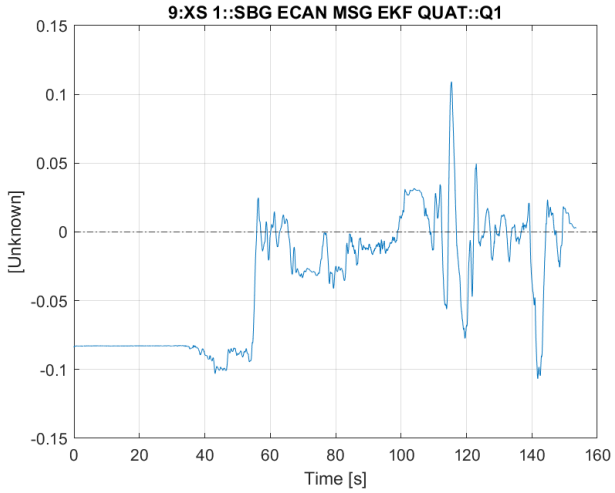

Figure 61 Quaternion 1

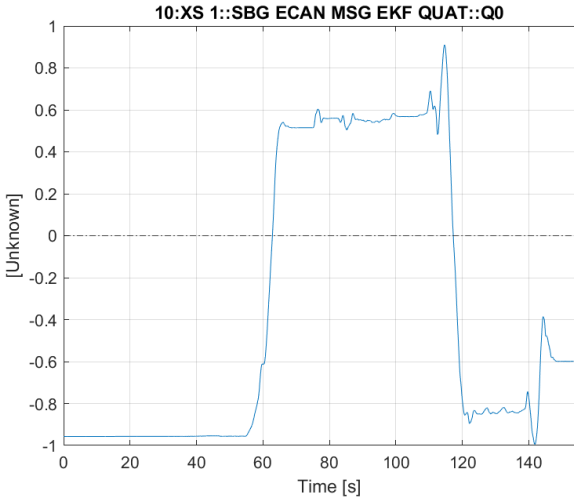

Figure 62 Quaternion 0

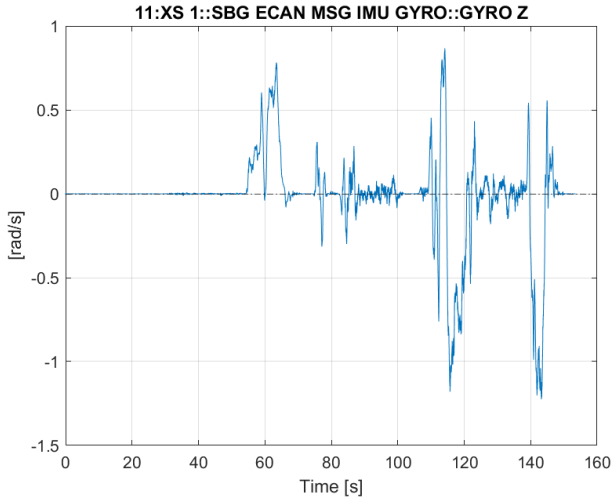

Figure 63 Gyroscopic signal, Z

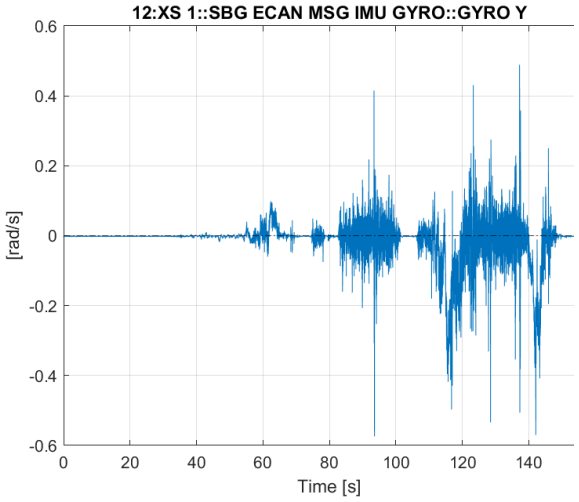

Figure 64 Gyroscopic signal, Y

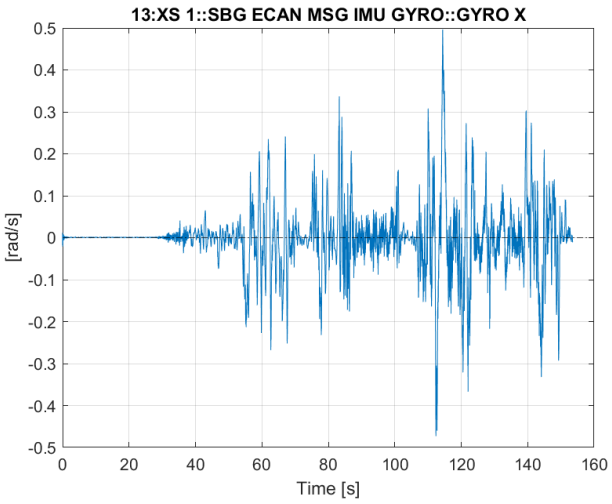

Figure 65 Gyroscopic signal, X

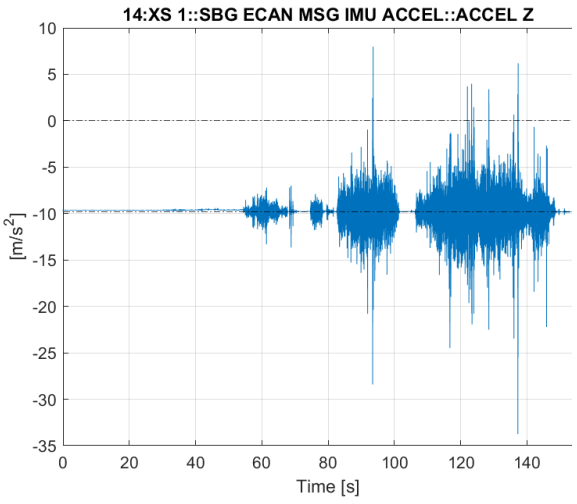

Figure 66 Acceleration signal, Z

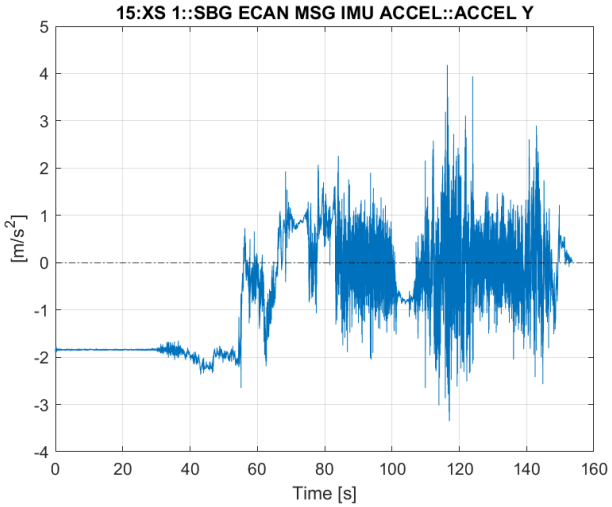

Figure 67 Acceleration signal, Y

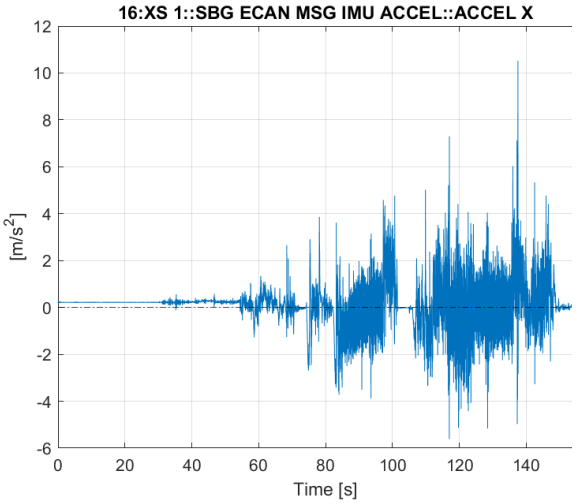

Figure 68 Acceleration signal, X

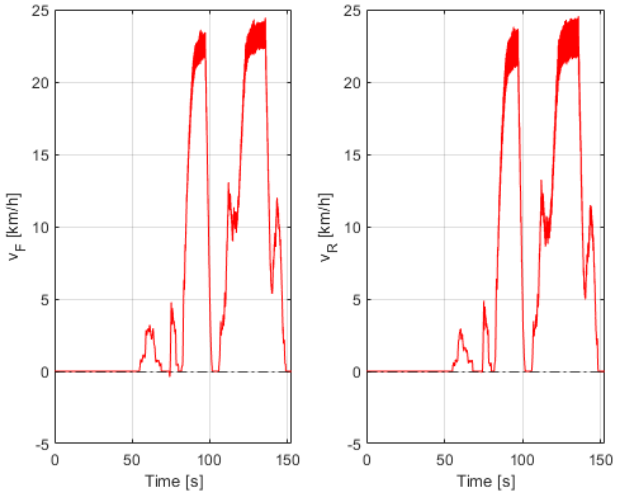

Figure 69 Front and rear linear velocities

Now, once the signals are retrieved and visualized, a resample is needed. Indeed, even if the majority of the acquisitions have been performed at a sampling rate equal to 200 Hz, a minority differs. The solution is so to resample such signals from their acquisition frequency to 200 Hz. In MATLAB, this is easily done by creating an array of elements corresponding to the desired sampling timestamp and by interpolating it with the original function.

Once again, some structs are built in order to store the information outside the cycle. In the 16th case, it is also represented an arrow pointing at the -9.81 m/s^2 threshold, indicating on the vertical acceleration plot the starting point (Figure 81).

Indeed, the constant vertical acceleration introduces an offset that could be simply removed by simply subtracting the gravitational acceleration value to the entirety of the array. However, it was decided to maintain it to show the real sensors reading.

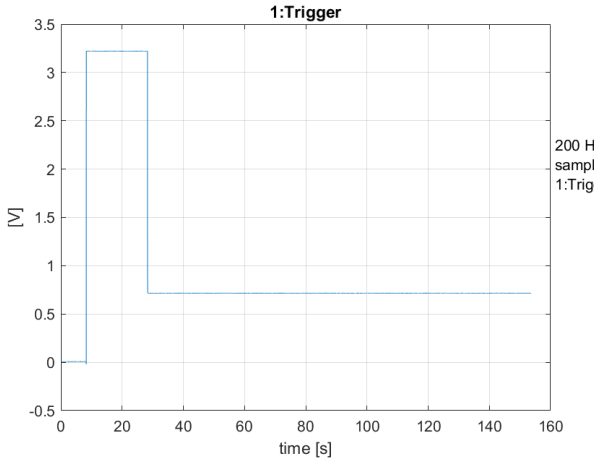

Figure 70 Trigger, resampled

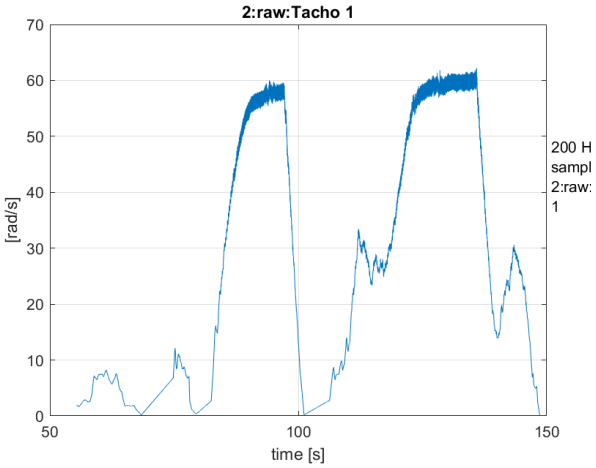

Figure 71 Raw front, resampled

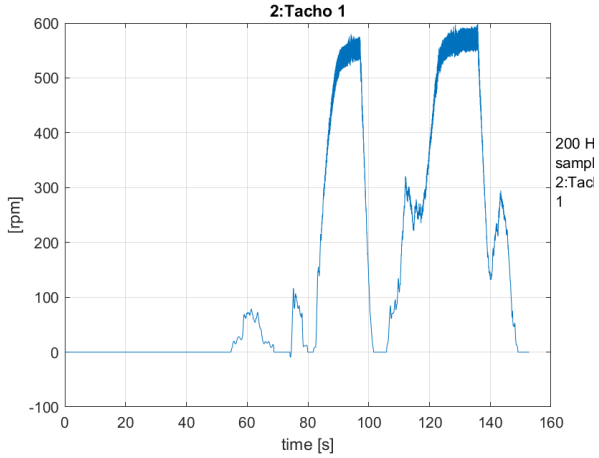

Figure 72 Front tachometer, resampled

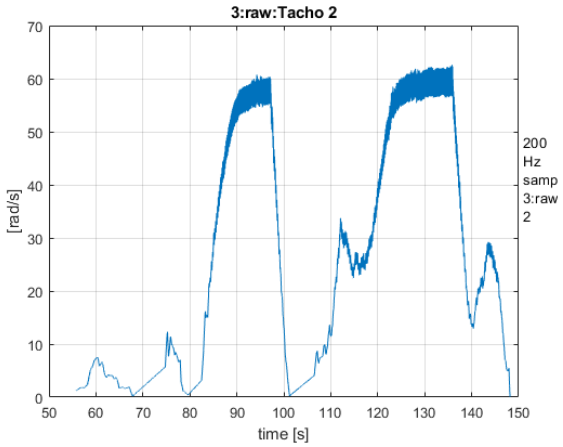

Figure 73 Raw rear, resampled

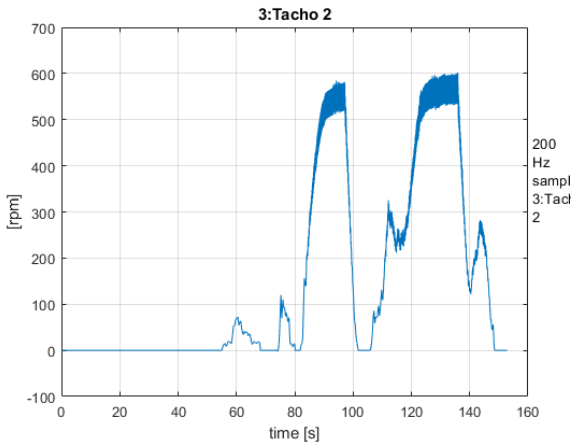

Figure 74 Rear tachometer, resampled

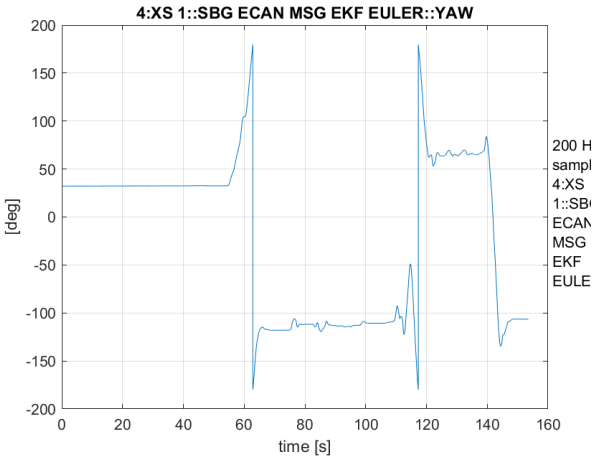

Figure 75 Yaw, resampled

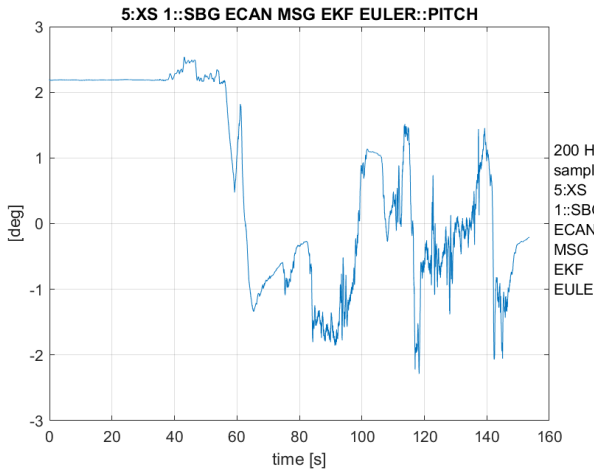

Figure 76 Pitch, resampled

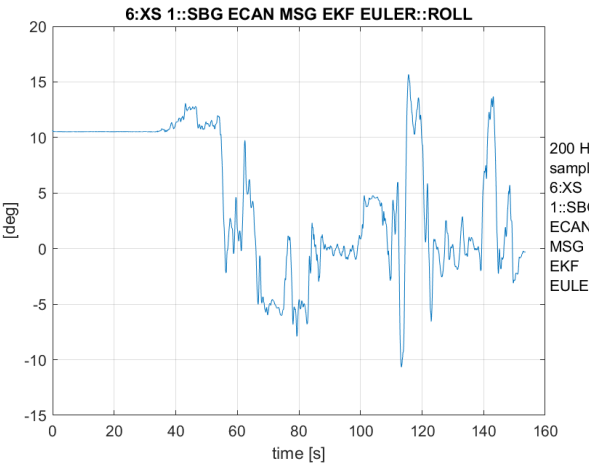

Figure 77 Roll, resampled

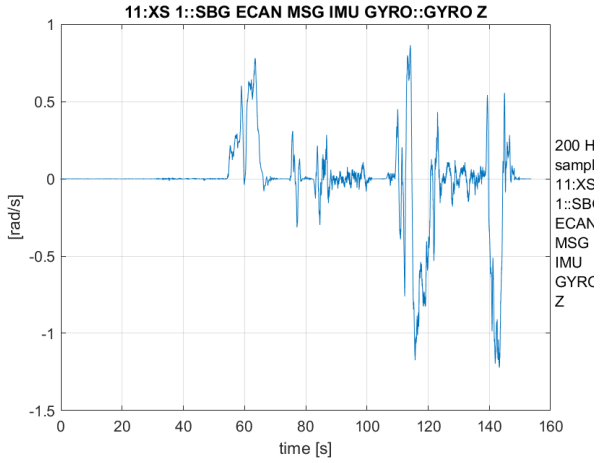

Figure 78 Gyroscopic Z, resampled

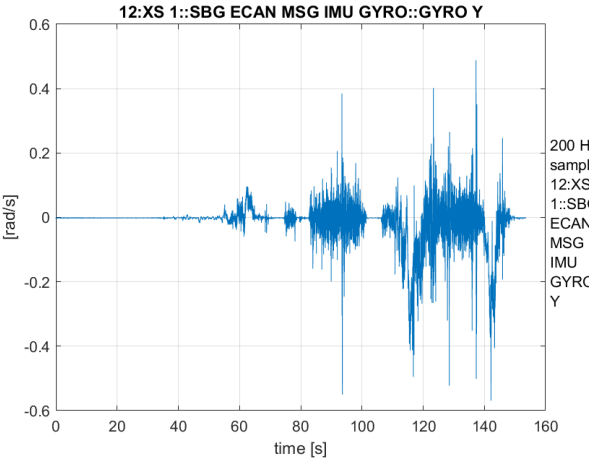

Figure 79 Gyroscopic Y, resampled

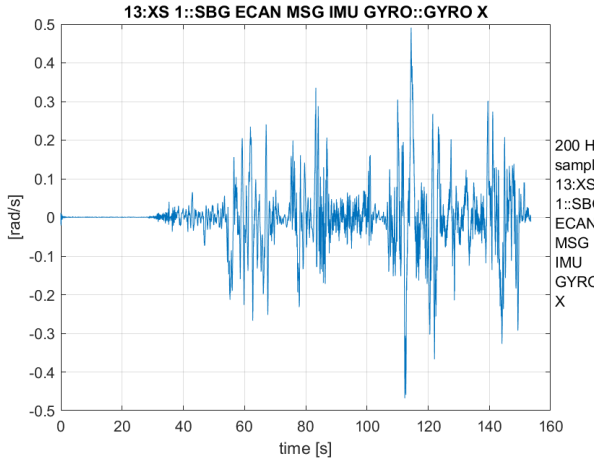

Figure 80 Gyroscopic X, resampled

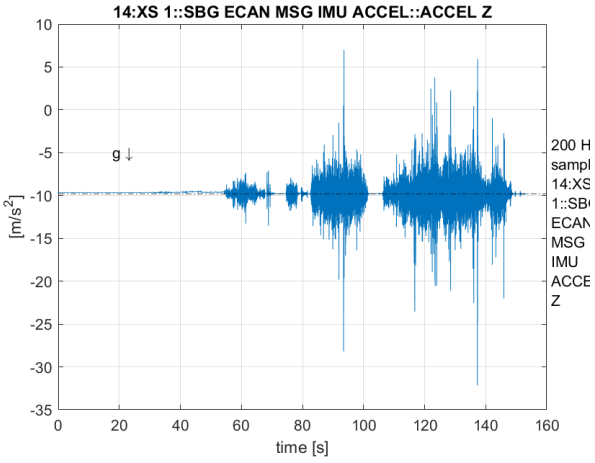

Figure 81 Vertical acceleration, resampled

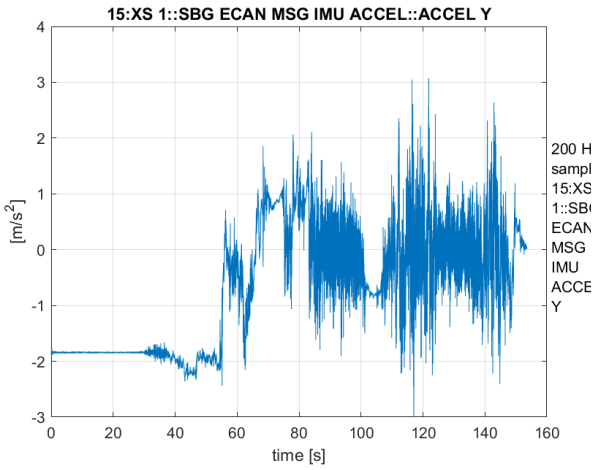

Figure 82 Lateral acceleration, resampled

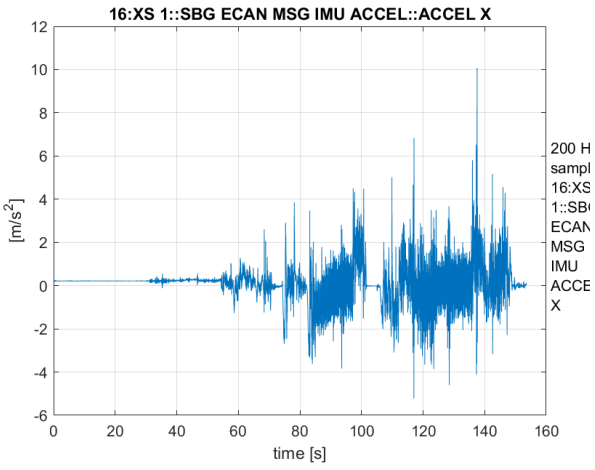

Figure 83 Longitudinal acceleration, resampled

After this considerations, by following the same procedure abovementioned, a comparison between the front and rear wheel velocities is performed both with the original raw signals and with the resampled raw signals (Figure 84 and Figure 85).

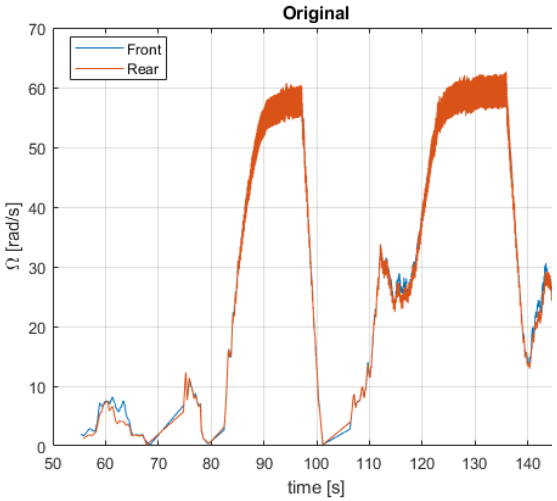

Figure 84 Original raw signals

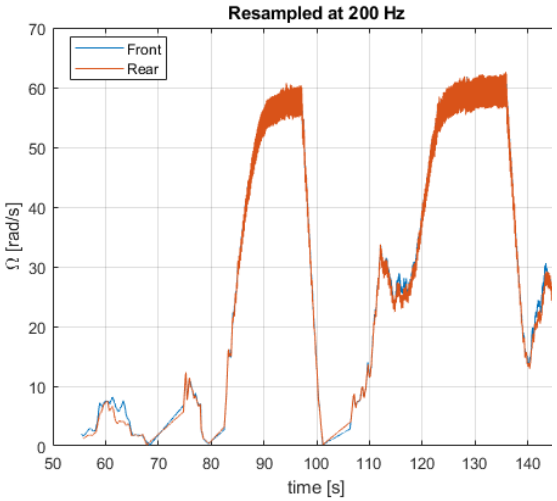

Figure 85 Resampled raw signals

By plotting and superimposing the front and rear velocities, the effect of the slip can be appreciated, having higher positive peak for the front wheel in the points of maximum torque (indeed, the e-scooter is by nature a FWD vehicle).

This preliminary analysis, focused on the longitudinal dynamic, shows the most important signals and information that need to be acquired to start the understanding of the vehicle as a whole. In order to enhance this understanding, along with this type of analysis, the information about the steering angle can significantly improve the outcome of the study. Indeed, the simple addition of such a reading can complete the data set introducing the only missing dynamic, the lateral one.

Being the setup completely manufactured and mounted, it is only a matter of time to be able to acquire, process and analyse the additional information.

After the present publication, documentation will report the employment of such setup and its contribution in an experimental campaign of testing.

8 Conclusions

The design phase underwent through a lot of changes, modifications and revisions. Every aspect of the setup was put under critical analysis to achieve the craved results: from the choice of the materials and their manufacturing, through the study of the most convenient kinematics, the assembly was defined.

In fact, as it can be seen from the previous chapters, even if at first glance it could seem the perfect solution, the pulley-style setup was later discarded in exchange for what was later realized. The choice was driven by the focus on the reliability in the readings and the possibility in fine tuning.

However, the final solution is to be considered as robust as it could, permitting to have a simple and cheap addition to the already present acquisition system, granting a solid reading of a quantity that strongly affects the dynamic behavior of a two-wheeled vehicle such as an e-scooter.

The relevance of this study relies on the importance of putting the right effort to achieve better understanding of dynamic phenomena that could alter the safety of the driving and affect the quality of the end-product.

Pursuing the goal to extend this approach to a vast fleet of 2WV, the setup was rearranged to adapt to another vehicle to be tested. Following the results obtained for the Xiaomi Pro 2 e-scooter, it was indeed decided to try to design a similar setup for an Aprilia ESR2 e-scooter.

The procedure was chosen as a carry-over from the previous design phase, starting so from the finding of a suitable mounting point for the assembly.

Once this point has been located, the couple of pieces devoted to the fixing of the system were sketched and implemented in CAD environment.

Having the mounts designed, it was time to proceed with the introduction of the biggest part of such a carry-over and to align properly the system composed by brackets, buttonhole, rod and potentiometer. The overall system can be seen in Figure 86 and in Figure 87.

Figure 86 Aprilia ESR2, lateral view

Figure 87 Aprilia ESR2, isometric view

A better view is then proposed to the reader in Figure 88 and in Figure 89.

To better visualize what has been added to the original vehicle, the additional components are highlighted in blue.

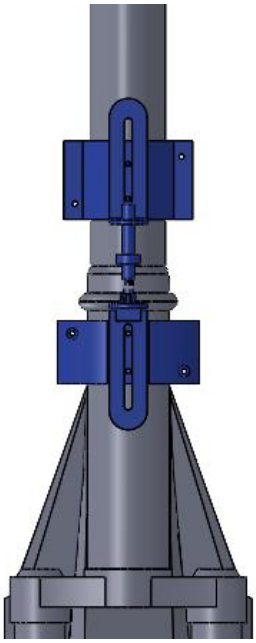

Figure 88 ESR2 setup

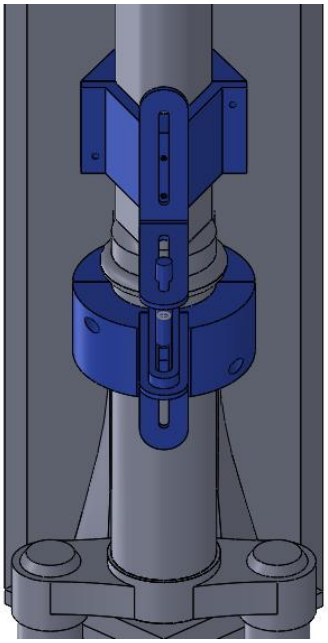

Figure 89 ESR2 setup, detail

As for what has been already done with the Xiaomi setup, the metal parts have been chosen to be produced by laser cutting, milling and lathe turning. The polymeric components instead, have been again destinated to additive manufacturing.

Noticeably, the same choices have been made also for the previous vehicle: this because they have shown to be the most practical ones, giving the best results at the minor cost in the least time, not introducing penalties in the process.

Although this system has not been yet implemented in reality, the outcome of the previous iteration permits to confidently believe that the solution can be considered robust and easy to manufacture and build. Further implementations will certainly be included in future publications.

Apart from these technicalities, It's almost frightening that no information is found regarding the lateral dynamics of e-scooters; moreover, it's even worse that neither the idea of trying to study such element has evidence of existing.

Surely the present document is intended to kick-start a different kind of approach to the final user care, focusing primarily on providing a well-studied product that could not lack of attention in important aspects as the one here treated.

Furthermore, the present thesis aims to be the basis for further in-deep investigations, starting with the adoption of similar systems to perform tests and experimental procedures to appreciate dynamics that were impossible to numerically address before.

In the hope to soon see the acquisition of the presented measuring system, the premises look very good, and surely further documentations will be redacted.

9 Appendix

9.1 Glossary of Symbols

Table 18 Symbols

δ	Steering angle	°
ϕ	Roll angle	°
ψ	Yaw angle	°
$\dot{\varphi}$	Roll rate	°/s
$\dot{\psi}$	Yaw rate	°/s
f	General frequency	Hz
p	Pitch	m
x	Longitudinal position	m
$\dot{x}$	Longitudinal velocity	m/s
$\ddot{x}$	Longitudinal acceleration	m/s^2
y	Lateral position	m
$\dot{y}$	Lateral velocity	m/s
$\ddot{y}$	Lateral acceleration	m/s^2
T	Steering torque	Nm

α	Experimental steering angle	°
β	Potentiometer shaft angle	°
V_B (V_{av})	Battery voltage	[V]
V_S	Scadas read voltage	[V]
γ	Partitioning factor	[-]
$\gamma_{L(R)}$	Partitioning factor at max left (right) turn	[-]
$V_{S,L(R)}$	Scadas read voltage at max left (right) turn	[V]
φ	Potentiometer angular range	[°]
$\varphi_{L(R)}$	Extreme potentiometer allowed angle, left (right) turn	[°]
V_{φ}	Voltage resolution over degree change	[mV/°]
df	Degrees of Freedom	[-]
SS	Sum of Squares	[-]
MS	Mean of Squares	[-]

9.2 Final Product: Pictures

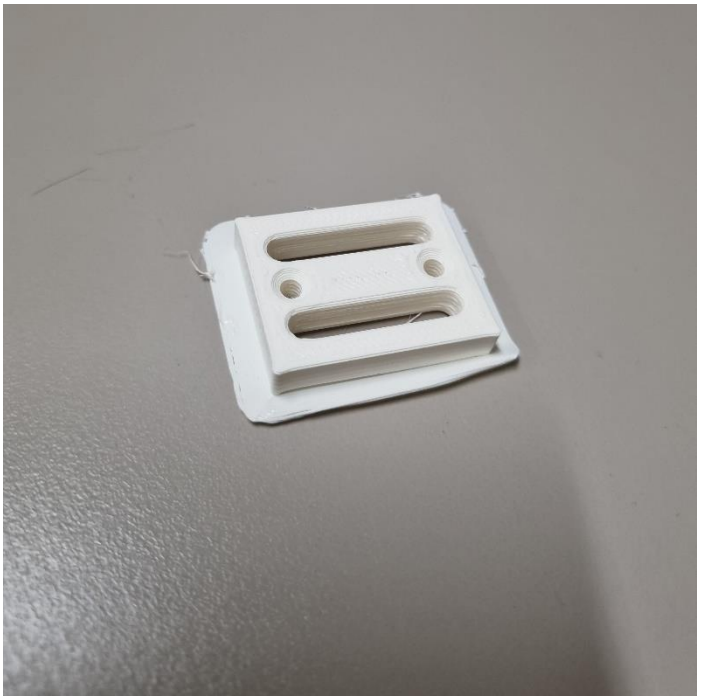

Support interfacing the main bracket to the mounts.

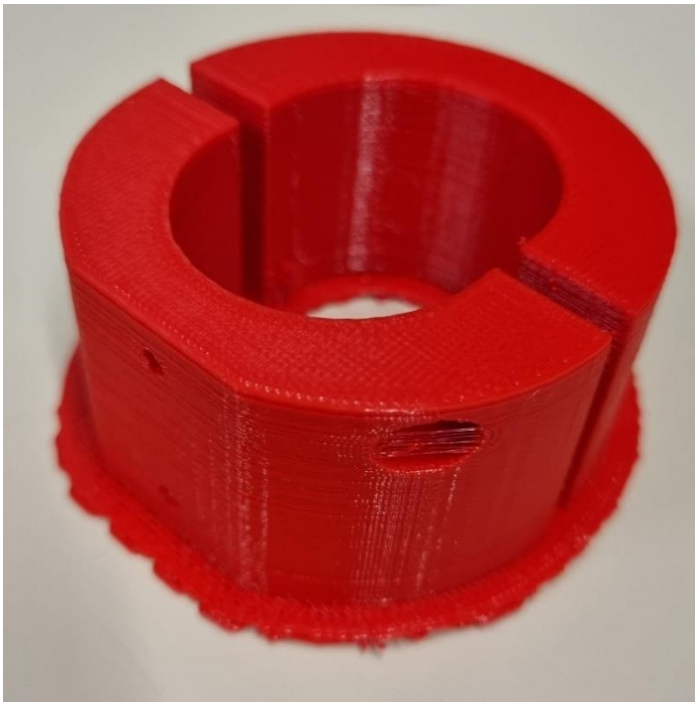

Mounts, raft included.

Mounts raft, detail.

Lateral view of the setup. Zero tuning.

Frontal view of the setup. Kinematic check.

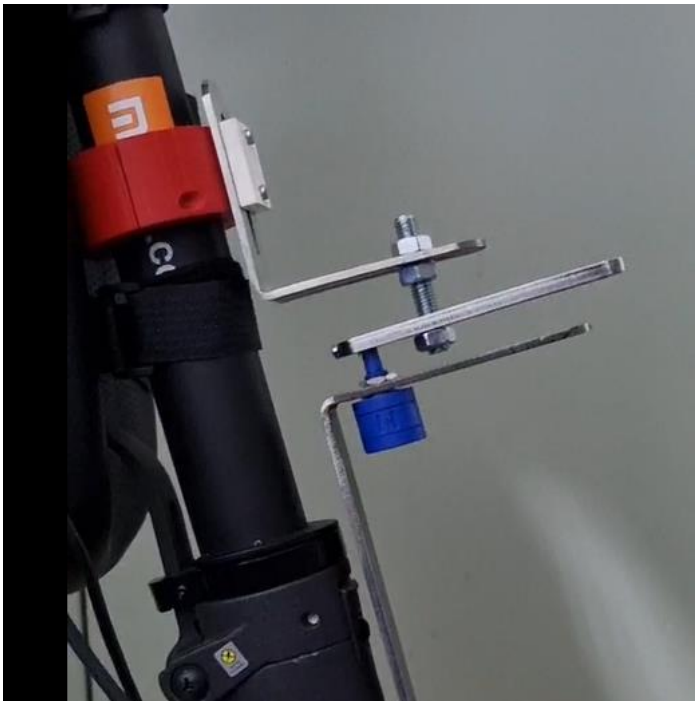

Lateral view of the setup. Tuned.

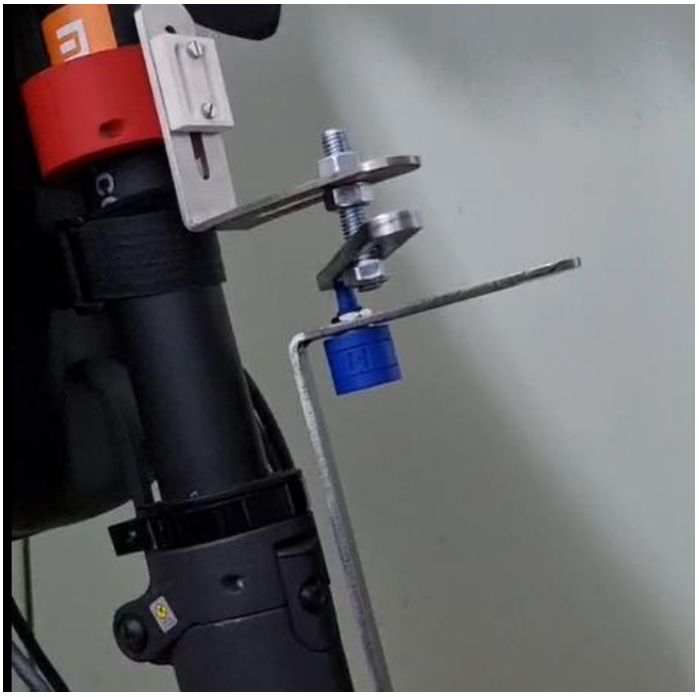

Lateral view of the setup. Kinematic check.

Top view of the setup.
Tuned.

Top view of the setup.
Kinematic check.

10 Reference

[1] A. D. Vella, «Electric kick scooter assessment from vehicle dynamics to rider perspective,» Torino, 2023.

[2] R. S. Sharp, «The lateral dynamics of motorcycles and bicycles,» 2010.

[3] M. K. Verma, «Theoretical and experimental investigations of motorcycle dynamics,» University Microfilms International, University of Michigan, 1978.

[4] S. H., A. H e M. S, «Motorcycle Lateral Dynamic Estimation and Lateral Tire-Road Forces,» in *ITSC 2013*, Netherlands, 2013.

[5] D. H. W. John W. Zellner, «Development of handling test procedures for motorcycles,» SAE International, 1979.

[6] R. Sharp, «The Lateral Dynamics of Motorcycles and Bicycles,» *Vehicle system dynamics: International Journal of Vehicle Mechanics and Mobility,* Vol. %1 di %214:4-6, pp. 265-283, 1985.

[7] F. Biral, D. Bortoluzzi, V. Cossalter e M. Lio, «Experimental Study of Motorcycle Transfer Function for Evaluating Handling,» *International Journal of Vehicle Mechanics and Mobilit,* vol. 39:1, pp. 1-25, 2010.

[8] F. Cheli, M. Bocciolone, M. Pezzola e E. Leo, «Numerical and experimental approaches to investigate the stability of a motorcycle vehicle,» in *8th Biennial ASME Conference on Engineering Systems Design and Analysis*, Torino, 2006.

[9] S. Singhania, I. Kageyama e V. M. Karanam, «Study on Low-Speed Stability of a Motorcycle,» 2019.

[10] P.-M. Damon, D. Ichalal e H. Arioui, «Steering and lateral dynamics estimation: validation of Luenberger LPV observer approach,» *IEEE Transactions on Intelligent Vehicles,* n. 2379-8858, 2018.

[11] A. Bonci, R. De Amicis, S. Longhi, E. Lorenzoni e G. A. Scala, «Motorcycle's lateral stability issues: comparison of methods for dynamic modelling of roll angle,» in *20th International Conference on System Theory, Control and Computing (ICSTCC*, Sinaia, 2016.

[12] «Docs,» 16 05 2017. [Online]. Available: https://docs.rs-online.com/5fbf/0900766b8169800f.pdf. [Consultato il giorno 20 11 2023].

[13] «Xiaomi Italia,» [Online]. Available: https://www.mi.com/it/mi-electric-scooter-Pro2/specs/. [Consulted on October the first, 2023].